NASA-CR-195933

Comprehensive Investigation of HgCdTe Metalorganic Chemical Vapor Deposition

Final Technical Report

Grant NAGW-1654

March 15, 1989 - March 14, 1993

National Aeronautics & Space Administration

Office of Space Science and Applications

submitted by

Arizona State University

Department of Chemical, Bio & Materials Engineering

Tempe, Arizona 85287-6006

Gregory B. Raupp, Principal Investigator

TABLE OF CONTENTS

1. SUMMARY

The principal objective of this experimental and theoretical research program was to explore the possibility of depositing high quality epitaxial CdTe and HgCdTe at very low pressures through metalorganic chemical vapor deposition (MOCVD). We explored two important aspects of this potential process: (1) the interaction of molecular flow transport and deposition in an MOCVD reactor with a commercial configuration, and (ii) the kinetics of metal alkyl source gas adsorption, decomposition and desorption from the growing film surface using ultra high vacuum surface science reaction techniques.

To explore the transport-reaction issue, we have developed a reaction engineering analysis of a multiple wafer-in-tube ultrahigh vacuum chemical vapor deposition (UHV/CVD) reactor which allows an estimate of wafer or substrate throughput for a reactor of fixed geometry and a given deposition chemistry with specified film thickness uniformity constraints. The model employs a description of ballistic transport and reaction based on the pseudo-steady approximation to the Boltzmann equation in the limit of pure molecular flow. The model representation takes the form of an integral equation for the flux of each reactant or intermediate species to the wafer surfaces. Expressions for the reactive sticking coefficients (RSC) for each species must be incorporated in the term which represents reemission from a wafer surface.

Because we were not able to determine accurate expressions for the sticking factors of metal alkyls used in CdTe or HgCdTe MOCVD, we used a published expression for the RSC of silane as a function of flux and wafer temperature developed from molecular beam measurements. Numerical solution of the resulting integral equation using Gauss-Legendre quadrature yields quantitative estimates of intrawafer film thickness uniformity for epitaxial silicon deposition from silane for specified process conditions and wafer radius:wafer separation. For given reactor dimensions and specified uniformity, throughputs can then be estimated.

The interactions of MOCVD precursors with Si and CdTe were investigated using temperature programmed desorption (TPD) in ultra high vacuum combined with Auger electron spectroscopy (AES). These studies revealed that diethyltellurium (DETe) and dimethylcadmium (DMCd) adsorb weakly on clean Si(100) and desorb upon heating without decomposing. These precursors adsorb both weakly and strongly

on CdTe(111)A, with DMCd exhibiting the stronger interaction with the surface than DETe. Dimethylcadmium partially decomposes to produce Cd adatoms; a large fraction of the excess Cd atoms desorb upon heating. In contrast, DETe desorbs without decomposing, suggesting that the rate limiting step in CdTe MOCVD on CdTe(111)A is surface decomposition of the tellurium alkyl. No evidence was found for alkyl radical desorption, although this pathway cannot be unequivocally ruled out. It appears that the carrier gas may play an important role in CdTe and HgCdTe MOCVD, in that adsorbed hydrogen atoms may facilitate decomposition of the alkyl by scavenging alkyls to produce volatile hydrocarbons which readily desorb. In the absence of significant overpressure of hydrogen, reaction rates under very low pressure conditions may be unacceptably low.

In terms of human resources development, this grant supported two graduate students during their thesis research. Dimitris A. Levedakis received his M.S. degree in Chemical Engineering in June 1991, and Mr. Wen-Shyrang Liu earned his Ph.D. in the Science and Engineering of Materials in December 1993.

The following publications resulted from the research described in this report:

(1) "Predicting Intrawafer Film Thickness Uniformity in an Ultralow Pressure Chemical Vapor Deposition Reactor", Gregory B. Raupp, Dimitris A. Levedakis and Timothy S. Cale, *J. Vac. Sci. Technol. A* 11(6), 3053 (1993).

(2) "The Surface Chemistry of CdTe MOCVD", Wen-Shyrang Liu and Gregory B. Raupp, *MRS Symposium Series*, in press (1994).

(3) "Modeling an Ultra Low Pressure Chemical Vapor Deposition Reactor", Dimitris A. Levedakis, M.S. Thesis, Arizona State University, June 1991.

(4) "Surface Chemistry of CdTe Organometallic Vapor Phase Epitaxy", Wen-Shyrang Liu, Ph.D. Dissertation, Arizona State University, December 1993.

2. PROBLEM STATEMENT AND REPORT OUTLINE

HgCdTe (MCT) based infrared detectors have a variety of exciting commercial and military applications. Commercial applications include fiber optic communication, infrared astronomy, scientific research in a variety of disciplines, and night vision. Military application include surveillance, target identification and tracking, as well as night vision. Utilization in these wide-ranging applications is limited by the prohibitive cost of high quality MCT crystals.

Metallorganic chemical vapor deposition (MOCVD) shows some promise as a relatively low cost technique for growing CdTe and MCT crystals. However, progress toward commercialization of this process has been slow. In this research we investigated several critical issues in CdTe MOCVD in an effort to better understand the limitations and underlying factors in implementing MOCVD under very low pressures.

Experience with epitaxial deposition of both elemental and compound semiconductors has shown that there are significant materials' quality advantages to deposition at low pressure and reduced temperature. One disadvantage of processing at these milder conditions is that low deposition rates are realized. From a practical viewpoint, there are several questions which must be addressed before low pressure epitaxial growth is a viable option. First, low deposition rates will require multiple wafer or substrate reactors to achieve reasonable production rates or throughput. The kinetics of the deposition process must be understood and ultimately controlled. The second question results from the first. Specifically, intrawafer or intrasubstrate film thickness uniformity will depend on a complex interaction between molecular flow or ballistic transport and heterogeneous reactions. An understanding of this interaction is critical to logical design and operation of low pressure MOCVD reactors.

In this report we document efforts to address these questions. Modeling of a very low pressure CVD reactor is described in Section 3 and Appendix I. The interaction of metal alkyls with silicon and CdTe surfaces using ultra high vacuum reaction techniques is described in Sections 4 and 5 and Appendix II. A bibliography of literature citations related to CdTe and MCT MOCVD is included as the first 92 references in the reference list [1-92].

3. MODELING OF VERY LOW PRESSURE CVD REACTORS

Meyerson and coworkers have experimentally demonstrated dramatic advantages to reduced temperature, ultra low pressure ($P \approx 0.001$ Torr) operation in chemical vapor deposition (CVD) of epitaxial silicon [93-95]. Silicon films deposited at ultra low pressures are essentially defect free and are of high purity [93,94]. Dopants can be incorporated to levels well above their solid solubility limits, and because of the relatively low deposition temperatures, junctions are abrupt [95]. Heteroepitaxial films and superlattice structures of SiGe are readily deposited [96]. An ultrafast heterojunction bipolar transistor has been fabricated using this technology to grow a boron-doped SiGe base region [97].

To realize these advantages, the reduced temperature and pressure process is performed in a custom designed ultrahigh vacuum reactor; for this reason Meyerson has called the process ultrahigh vacuum chemical vapor deposition (UHV/CVD). The clean environment allows surface silicon oxide and hydride contaminant layers to be removed *in situ* by a high temperature bake in vacuum prior to deposition [93,94]. The resulting oxide-free surface provides a high quality surface on which epitaxial silicon deposits from silane containing gas mixtures at temperatures significantly lower than conventional low pressure, cold wall epitaxial deposition processes (1023-1123 K versus 1273 K or greater). Growth of SiGe layers can be accomplished at even lower temperatures [96,98,99].

Although the use of reduced temperatures and pressures during deposition enhances material and device properties, throughput may be an issue in a production environment since these conditions also lead to significantly reduced deposition rates. Low throughput may be mitigated by employing load-locked wafer handling and a volume-loaded multiple wafer-in-tube hot wall reaction chamber [95,94,98]. To maximize throughput in such a reactor, wafer spacing and reaction conditions must be chosen to maximize deposition rate while meeting intrawafer and interwafer film thickness uniformity constraints. This problem has been discussed previously for low pressure CVD reactors by Jensen and Graves [100].

To assist efforts in optimizing operations of UHV/CVD reactors, we present a detailed mathematical model of reactant transport and deposition in the interwafer space in a multiple wafer-in-tube reactor. This model differs significantly from that of Jensen and Graves, since transport between wafers is by molecular flow. Thus the continuum dynamics descriptions of gas flow represented by the Navier-Stokes equations must be

replaced by the Boltzmann transport equation and the Kinetic Theory of Gases. We present a model representation of transport and reaction within the space between the wafers which takes the form of integro-differential equations for the flux of the reactant or intermediate species to the wafer surfaces. For established heterogeneous deposition kinetics, the model contains no adjustable parameters. We have illustrated the predictive capabilities of the model for epitaxial silicon deposition from silane. A paper documenting the model has been published in the Journal of Vacuum Science and Technology; a reprint of this paper can be found in Appendix I.

4. EQUIPMENT AND EXPERIMENTAL PROCEDURES

A. Equipment

The temperature-programmed desorption (TPD) experiments on CdTe and Si substrate surfaces were performed in a bakeable, stainless-steel, ultra high vacuum (UHV) chamber which was pumped by a Perkin-Elmer TNB-X vacuum system (base pressure about 2 x 10^{-10} Torr). The UHV chamber was equipped with a Perkin-Elmer retarding field Auger Electron Spectrometer (AES) and a VG SX 300 Quadrupole Mass Spectroscopy (QMS). An IBM compatible computer is used to perform TPD in a Multiple Ion Monitoring mode, and to record the temperature of the sample. Gas dosing of hydrocarbon and metalorganic gases was accomplished through a specially designed two-cylinder expansion volume system. The sample is heated radiatively and is cooled by thermal conduction between the crystal holder and a liquid nitrogen reservoir.

i. Vacuum Chamber and UHV Pumping

The stainless steel ultra high vacuum chamber was custom-designed to incorporate a variety of bolt-on vacuum components. The physical arrangement of the principal components is shown schematically in Figure 4-1.

Ultra high vacuum conditions provide several advantages in the study of gas-solid reactions which can not be realized in higher pressure circumstances: (1) Sample surfaces can be well controlled. In UHV atomically clean surfaces of desired composition and structure can be prepared and retained. (2) In situ UHV surface analysis techniques permit structural and compositional characterization of these surfaces before and after operation. (3) TPD experiments can be carried out under conditions such that gas-phase diffusional limitations, homogeneous reaction and readsorption are negligible. As a consequence, intrinsic surface processes can be directly examined.

The UHV chamber is pumped by a Perkin-Elmer TNB-X vacuum system. The TNB-X vacuum pumping system includes two sorption pumps, a differential ion pump with a poppet valve, a titanium sublimation pump interfaced through the digital ion pumping controller and the titanium sublimation supply control unit. The combination of these pumps made it possible to routinely obtain a base pressure of 2 x 10^{-10} Torr.

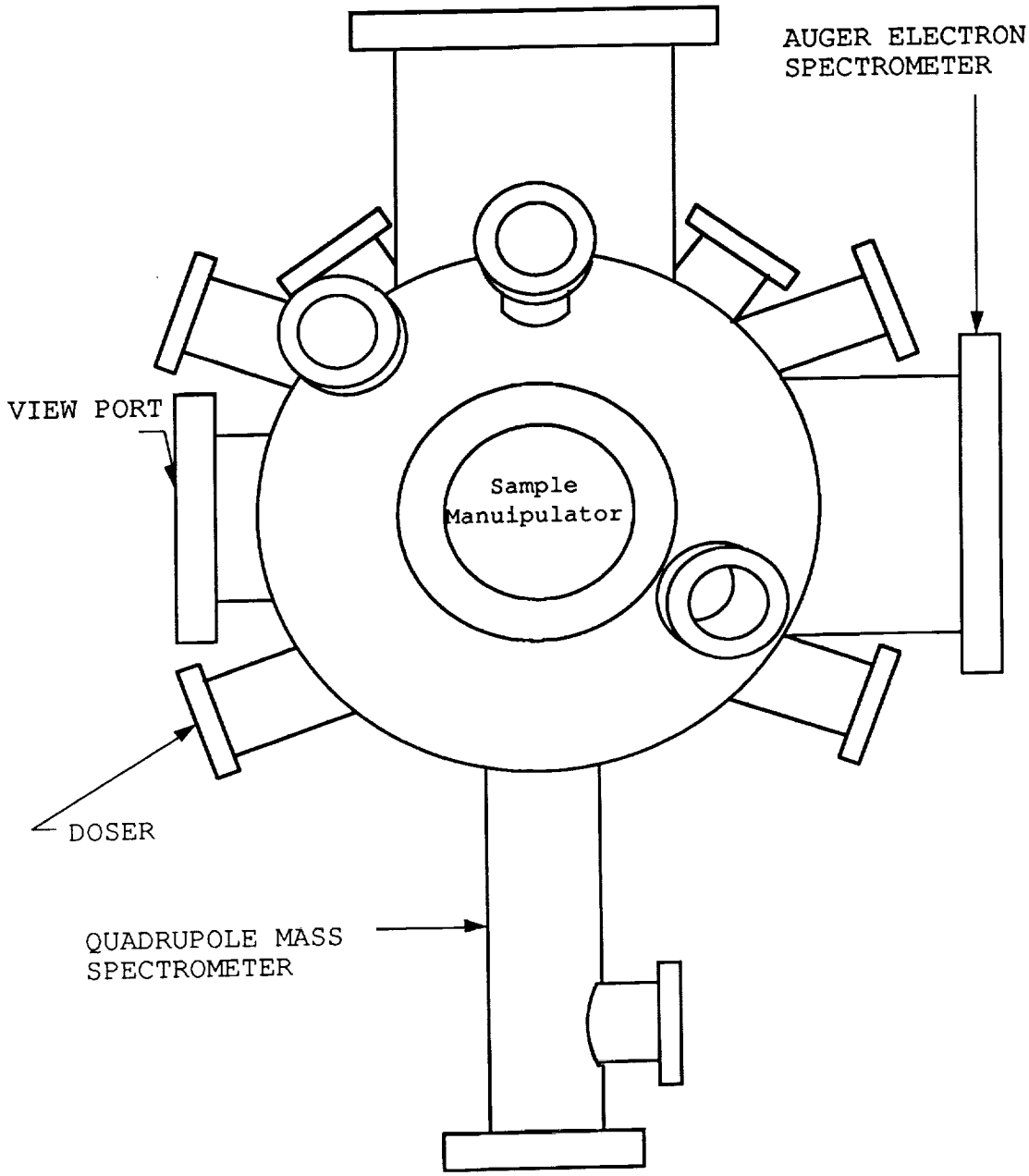

Figure 4-1 UHV Chamber

The first stage of a two-stages cryosorption pump manifold is used to rough to 10^{-1} Torr within 2.5 minutes; the pump is then quickly valved from the manifold and the second stage is used to pump to 10^{-3} Torr or lower range within 7.5 minutes. The pressure at this stage was measured by a Granville-Phillips thermocouple vacuum gauge. The sputter ion pump can be cold-started when the chamber pressure reaches 10^{-3} Torr or lower pressure.

Ultra high vacuum was reached using a 200 liters per second (lps) sputter-ion pumping augmented by a 200 lps titanium sublimation pump. The UHV chamber was capable of $2x10^{-10}$ torr as measured by a Bayard-Alpert ionization gauge.

Operation of the TNB-X vacuum pumping system is as follows:

(1) Sorption pumping to obtain rough vacuum of about 10^{-3} to 10^{-4} Torr.
(2) Ion pumping to obtain vacuum in the range of high vacuum to ultra-high vacuum of about 10^{-8} Torr.
(3) Baking at 150°C for 48 hours to achieve UHV conditions.
(4) Titanium sublimation to supplement ion pumping.

After rigorous outgassing of all metal parts of the chamber, the pressure typically fell to a limiting value of 2 X 10^{-10} Torr. The residual gases (vacuum quality) in the UHV chamber were analyzed by quadrupole mass spectroscopy; typical analyses revealed that the background was found to contain 5% H_2, 1.5% Ar, 3% CO_2, 40% CO, 23% H_2O, 23.5% simple hydrocarbon gases.

ii. Auger Electron Spectroscopy

A Perkin-Elmer LEED-AUGER unit, model PHI 15-180 is employed to collect retarding field Auger spectra. The incident electron beam pass along the axis of the optics, striking the sample at normal angle. The retarding field analyzer[101,102,103] employs four concentric grids and a collector. The first grid (nearest to the sample) , is grounded as are the sample and all neighboring components, in order to give an electrical field-free region between the grid and sample. This arrangement guarantees that emitted Auger electrons at the center of curvature of the optics will travel in a radial path toward the first grid. The next two grids are retarding grids which stop electrons with energy below a set value from passing them. Two grids of this kind are used in order to sharply define the radial retarding field, and to obtain a high energy resolution. An AC modulation voltage is applied to these two grids together with the DC retarding field, enables energy analysis to be

carried out. The fourth grid is held at ground potential and serves primarily as an AC shield to reduced the capacitive coupling to the collector of the AC voltage applied to the retarding grids. The collector is a fluorescent screen biased at 180 volts with respect to ground.

When the sample is stimulated by primary electrons of energy E_p and the current to the collector is recorded as a function of the retarding field voltage, sweeping from ground potential to the potential of the cathode, a retarding field plot is obtained. Automatic differentiation is accomplished by applying a small AC modulation voltage to the second and third retarding grids and tuning the detector to the frequency of the modulation. In order to obtain the derivative of the energy distribution curve, the detector is tuned to the second harmonic of the modulation frequency. Peaks at characteristic Auger electron energies permit determination of the elemental composition of the surface of the sample, including adsorbed molecules on the surface. Quantitative analysis may be accomplished with varying degrees of accuracy by comparing the peak heights obtained from an unknown specimen with those from pure elemental standards or from compounds of known composition. When no standards and known composition compounds are used, the atomic concentration is usually expressed as:

$$C_x = \frac{I_x}{S_x\, d_x} \Big/ \sum_{\alpha} \frac{I_\alpha}{S_\alpha\, d_\alpha}$$

where I_x is the peak-to-peak amplitudes from the Auger spectrum, S_x is the relative sensitivity (values can be obtained from the standard Auger spectra in the handbook[104]), d_x is the scale factor; a function of modulation energy, primary beam current and the gain of the lock in amplifier. When the experimental conditions are kept the same, the scale factor will be the same for all peaks and therefore cancels out. Since the low energy Auger peaks are more sensitive to sample charging problems, it is better to select peaks occurring above about 100 eV for quantitative analysis.

iii. Quadrupole Mass Spectroscopy

Quadrupole mass spectroscopy (QMS) provides the capability of simultaneous identification of the components of the gas under analysis. In this work, a Vacuum Generators' SX 300 RF quadrupole is employed. A secondary electron multiplier (SEM) is used to detect ion signals ranging from a single ion to 10^{-9} A. The advantages of the secondary electron multiplier

are its high sensitivity and rapid response. The disadvantage of the secondary electron multiplier is that the statistical probability of an electron being released when the multiplier is knocked by an ion is less then one. Since it is well known that electronic component will change with time, calibration must be performed periodically. In addition, if the equipment has been moved, the high mass resolution must be calibrated. In this laboratory, argon (m = 40) and xenon (m = 132) were used as calibration gases for low and high mass ranges, respectively. Argon gas (99.9995 %) was obtained from Liquid Air Corporation[109]. Xenon gas (99.9995 %) was obtained from Spectra Gases,Incorporated[110].

iv. Dosing System and Capacitance Manometer

For this work a custom dosing system was designed so that the gas to be adsorbed on the sample located in the UHV environment could be introduced in a controlled manner. The system was designed so that the background pressure in the UHV chamber could be kept between 10^{-8} and 10^{-10} Torr during dosing. The nature of the metalorganic source gases posed special problems which required a flexible, safe design. In particular, the sources normally exist as liquids at room temperature, and they have substantially different vapor pressures. Safety is the highest priority, since the threshold limit valve (TLV) of the metalorganic gas is very low, the metalorganics are pyrophoric and spontaneously flammable in air, and the usual fire - extinguishing agent, halon, is not suitable for metalorganic gas fires.

Figure 4-2 is a schematic diagram of the hazardous gas dosing system. The dosing gas manifold is constructed entirely of 1/4 inch diameter seamless stainless steel tubing with Nupro relay and pneumatically operated valves and VCR fittings with metal gaskets. A cylinder of nitrogen is provided for purging the whole system when the electrical power is suddenly shut off. In our case, the purge gas used is 99.99% nitrogen, but any gases such as argon or helium which do not react with the metalorganic gas could also be employed. The source bottle[111] is specially designed for MOVPE, and has three openings: the inlet opening is used for entering carrier gas, the fill port is used for filling the metalorganic gas, and the outlet opening. The metalorganic gas cylinder is immersed in a slurry bath - dewar with dry ice to control the source vapor pressure and the vapor in equilibrium over the liquid is withdrawn through the outlet tube. The manifold is connected to two 1-liter evacuated reservoirs. By using a combination of these expansion volumes, a desired pressure can be obtained in the second cylinder. The pressure of the dosing species in this

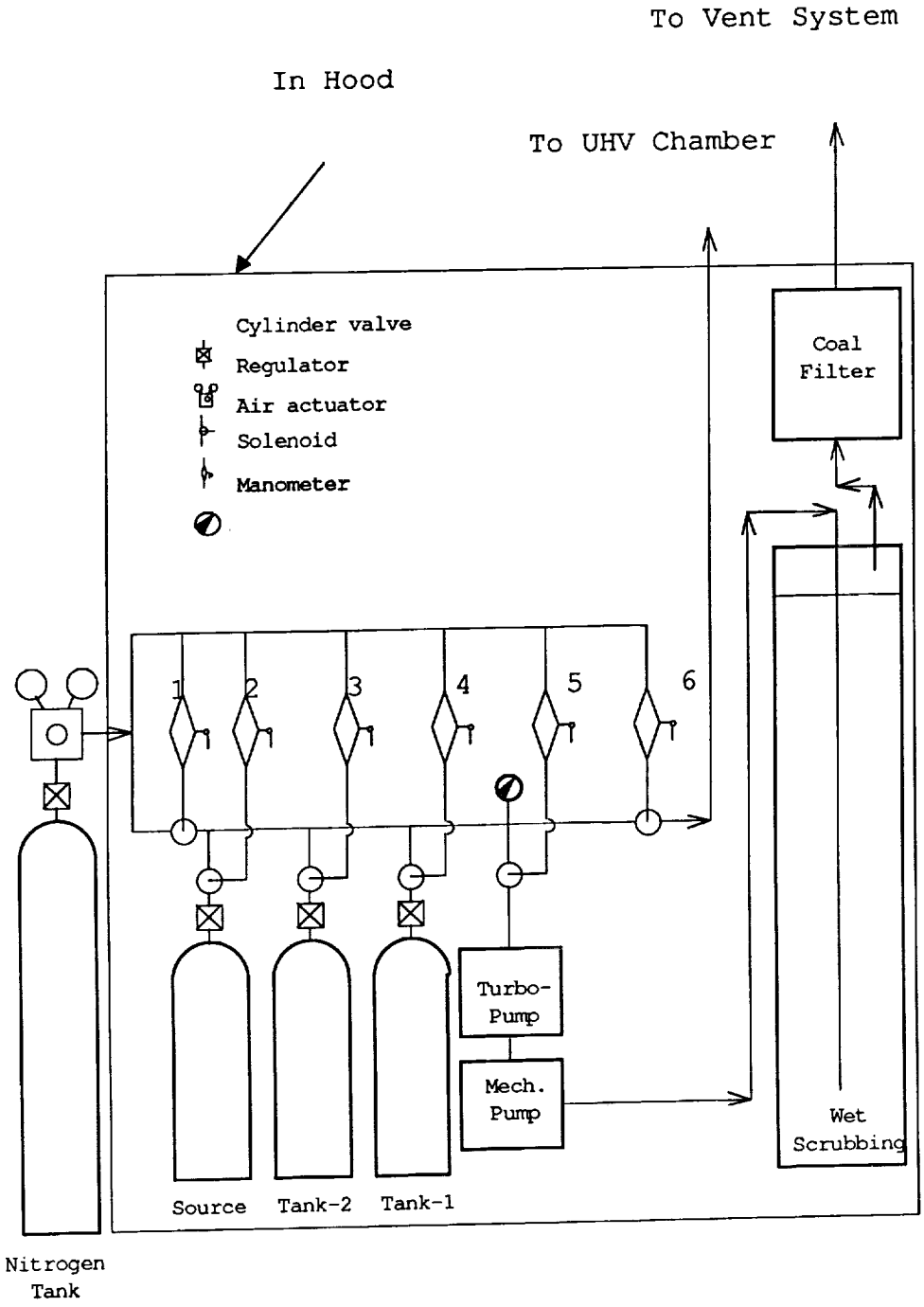

Figure 4-2 The Dosing System

reservoir is kept below its vapor pressure to prevent condensation near the working part of the leak valve. Therefore, for dosing species with low vapor pressures only a small pressure of the desired species is possible in the reservoir upstream from the leak valve. A Varian turbopumping system was used to evacuate the manifold prior to use. Unused gases were pumped from the system and piped to a wet gas scrubber. Metalorganic gases react with sodium hypochlorite solution (NaClO) in the scrubber to produce relatively non-toxic products through chlorization and hydrolysis reactions. The exhaust line was fitted with a disposable activated charcoal filter to absorb final traces of metalorganic gas from the exhaust line.

A capacitance manometer is used to measure pressure in the manifold. The manometer yields an absolute-pressure measurement in the range of 1 mTorr to 10 Torr.

The manifold is connected to a UHV precision stainless steel leak valve that is mounted on a flange of the UHV chamber. A pinhole doser on a 1/4 inch diameter tube was used to direct the gases passing through the leak valve directly onto the substrate.

The dosing system was pressure-tested to 500% of source pressure and helium leak-checked to a level of 10^{-8} Torr. The entire dosing equipment was housed in an extracted flow hood.

B. Sample Preparation and Experimental Procedures

i. Cadmium Telluride Sample Preparation

Single crystals of p type CdTe (111), 16 Ω-cm, grown from the melt , purchased from II-VI incorporated[112], were employed. Experiments were performed to find a reproducible method for obtaining a nearly atomic-clean surface of CdTe in situ. The literature reports several reducing and oxidizing treatments which have been applied to chemically treat the CdTe surface. Table 4-1 summarizes the most commonly used chemical etches for CdTe.

In this research the crystal was cleaned by immersion in E-solution ($K_2Cr_2O_7$ 4g, HNO_3 10 ml, H_2O 20 ml) for 30 seconds and in dithionite solution (0.6 M $Na_2S_2O_4$ and 2.5 M NaOH) 1-3 minutes at boiling temperature. The sample was subsequently loaded in the UHV chamber within 30 minutes.

Table 4-1. The Commonly Used Etches for CdTe

Etching solution	Composition	Action
E Solution[113]	$K_2Cr_2O_7$ - 4 g HNO_3 - 10 ml H_2O - 20 ml	At room temperature for 30 s
Chemical etching	Br 4 vol % in MeOH	At room temperature
Nakagawa Solution[114]	HF - 30 ml H_2O_2 - 20 ml H_2O - 20 ml	At room temperature
Hydrazine[115]	N_2H_4 - 95% solution	At room temperature for 5 minutes
Dithionite solution[115]	$Na_2S_2O_4$ - 0.6 M NaOH - 2.5 M	At boiling temperature for 1-3 minutes

The hydrogen heat treatment[116] was performed by exposing the sample at fixed temperature of 450°C to ultra pure hydrogen gas. After heat treatment, the CdTe sample was annealed in vacuum at 350°C for 30 minutes. The impurities on the CdTe (111) surface were checked by AES. Typically less than 10 atom % of carbon and sulfur impurities were present. No detectable oxygen Auger signal was evident after hydrogen heat treatment. The AES spectra are shown in Section 5.

ii. Silicon Sample Preparation:

Silicon samples were cut from silicon wafers with p-type bulk doping (r = 1 ~ 10 Ω - cm). Before loading the sample into the UHV chamber chemical etching steps were applied to remove contaminants and to remove the impurity of the thin nature oxide layer.

The following procedure was used to etch silicon samples[117]:

1) Place 50 ml of 30% H_2O_2 in a clean beaker
2) Place the sample in the beaker
3) Carefully add 30 ml concentrated H_2SO_4
4) Gently agitate for 2 minutes
5) Decant
6) Rinse with deionized water, repeat 5 times
7) Place 1/4 to 1/2 inch of 50% HF in a shallow wide mouth teflon beaker
8) Using teflon tweezers push the sample into the HF
9) wait 30 to 60 seconds then remove sample.

After removal from the HF, the sample should be totally hydrophobic. If this is not the case the whole procedure was repeated.

To prepare an atomically clean silicon surface in UHV vacuum annealing was employed. Standard contaminants on Si samples are oxygen and carbon, which are readily monitored using their Auger lines at 510 and 272 eV, respectively. Oxygen forms silicon oxide, which sublimes at 800°C. Carbon forms silicon carbide, which never goes away, but does coalesce into large islands at ~ 1200°C. After transferring the Si sample into the UHV chamber, the oxide layer was removed by heating the sample in UHV to temperatures between 800 and 900 °C for 2 minutes. The cleaned Si surface was analyzed by Auger electron spectroscopy (AES); results are shown in Section 5.

iii. Sample Arrangement:

The sample was mounted on a rotary feedthrough, which includes two-copper conductor feedthroughs (25 volts, 40 ampheres) , a two-tube liquid nitrogen feedthrough, and a 3-pairs thermocouple feedthrough to aid in heating, cooling, and measuring the temperature of the sample, respectively.

The sample, 20 mm by 12 mm, was clamped to a small stainless steel plate by 4 tantalum (Ta) tabs. The small plate was mounted on the rotary manipulator by two stainless steel bolts but separated by 2 sapphire rings. One side of the sapphire rings was in contact with the liquid nitrogen reservoir, the other side was in contact with the bottom of the stainless steel plate. This arrangement allowed thermal conduction cooling of the sample and electrical isolation from the rotary manipulator, because the sapphire is an electrical insulator with good thermal conductivity. Tungsten wire of 0.508 mm in diameter wound into a flat spiral coil approximately 10 mm in diameter area was used as the radiation heating coil. This heating coil was connected to a pair of copper leads and positioned 2 mm behind the sample. The heating coil was heated using a 0 to 40 volts, 0 to 25 amp DC power supply (Hewlett-Packard, model 6434B). CdTe and Si samples typically required 10 to 16 A to produce heating rates of 5 to 15 K/s. Sample cooling to 120 K was achievable by thermal conduction through the two sapphire rings to the stainless steel plate cooled by liquid nitrogen. Through this arrangement, sample cooling from 675 K to 150 K could be achieved in 25 minutes. The temperature of the sample was monitored continuously with a nickel-chromium versus nickel-alumel thermocouple (0.076 mm diameter) spot-welded to a piece of tantalum (Ta) thin foil clamped to the sample.

iv. TPD Data Collection

In typical experiments, the sample is exposed to a known gas. After the desired exposure, the UHV chamber was pumped down to the base pressure of the UHV system. When the sample is heated to desorb the gas from the sample, the pressure and the temperature in the system were recorded as a function of time. Because this system has high pumping speed, the signal of the quadrupole mass spectrometer is directly proportional to the desorption rate from the substrate surface.

The quadrupole mass spectrometer (QMS) was connected to an IBM compatible computer by means of a SensorLab interface. Temperature programmed desorption (TPD) spectra

were collected in a Multiple Ion Monitoring (MIM) mode and stored for subsequent computer analysis. All TPD results are presented in color graphics on the monitor simultaneously and also be stored in computer hard disk. A recipe specifying the mass, detector type, signal range, cycle-period for each channel, was constructed before TPD experiments. A total of 16 mass spectrometer channels to be selected for analysis and 2 analog inputs were available. The output consists of a mantissa which is measured as the amplifier output from 0 to 10 V, and an exponent which depends on the signal range set in the recipe. The thermocouple signal was amplified to provide 0 to 10 DC volts as required by the analog to digital converter. The amplifier, designed and built by ASU Engineering Laboratory Service, has a gain of approximately 400 and was linear over the experimental range from -150 to 350^{0}C. Cracking patterns for the metalorganic gases under consideration were experimentally determined and used to deconvolute desorption spectra possessing signal overlap from more than one mass fragment. Cracking patterns for the common hydrocarbon gases under consideration were checked from the VG - cracking pattern calculator.

A conversion utility program named " POST " is executed from DOS and can convert the Multiple Ion Monitoring (MIM) files to ASCII files. Then the transferred ASCII file can be directly imported into a computer spreadsheet program, for example, SuperCalc 4 for IBM PC computers or EXCEL for Macintosh computer systems. When the ASCII file is presented in the spreadsheet the data can be manipulated to meet the analysis requirement.

5. RESULTS AND DISCUSSION

The interactions of simple hydrocarbons and II-VI precursors with well characterized cadmium telluride (CdTe) and silicon (Si) single crystal surfaces have been investigated using temperature programmed desorption (TPD) techniques. The results of these studies are presented and discussed in this section.

All experiments were carried out in the ultra high vacuum chamber with VG SX 300 quadrupole mass spectroscopy (QMS) and conventional four grid LEED-AES system described in Section 4. In general, a series of TPD experiments with different gas doses was performed for each surface-gas combination. The dosing range varied from 21 L to 2.3 $x10^4$ L (1 Langmuir = 10^{-6} Torr-sec). In most experiments, the substrate temperature during dosing was held at about 120K. The heating rate is approximately linear ($T = T_0 + \beta t$). The value of β ranges from 8 to 17 K/s depending on the sample and experiment set. During experiments the instantaneous substrate temperature and the ion fluxes of the cracking fragments of the dosing gas were automatically recorded using a computer controlled quadrupole mass spectrometer. Desorption spectra were constructed by plotting the ion currents as a function of substrate temperature. Further analysis yields defining process parameters, such as the activation energy for desorption and the kinetic order.

A. Results

i. Interaction of Simple Hydrocarbons with CdTe

To quantify the strength of interaction of potential hydrocarbon reaction products with a growing CdTe layer and to facilitate the interpretation of the thermal desorption of sources gases, TPD spectra for simple hydrocarbons from cadmium telluride were obtained. The simple hydrocarbons methane (CH_4), ethane (C_2H_6) and ethylene (C_2H_4) are those commonly produced in metalorganic vapor phase epitaxy processes employing methyl and ethyl alkyl sources gases.

Single crystals of p type CdTe (111), 16 Ω-cm, grown from the melt , purchased from II-VI Incorporated[112], were employed. In order to clean the CdTe crystal surface, reducing, oxidizing and hydrogen heat treatments described in detailed in Section 4, Section B, were used. The treated surface was analyzed with AES using a 2950 V, 6 mA electron beam. The Auger electrons were analog plotted in the dN(E)/dE mode with modulation voltage = 6 V, time constant = 100 ms,

and sensitivity = 3 mV. Figure 5-1 shows an AES spectrum of the cleaned CdTe (111)A surface. Auger peaks indicate the presence of sulfur (152 eV), carbon (272 eV), and oxygen (510 eV) impurities. Peaks associated with cadmium are at 376, 382, 277 and 321 eV, and those for tellurium are at 483, 491, and 526 eV. Sulfur, the principal contaminant, originates from the etching solution. Carbon and oxygen are common surface contaminants. Based on published sensitivity factors[104], the total impurity is about 8 atomic %. The transition and relative sensitivity of some elements used in this work are listed in Table 5-1. The carbon peak (272 eV) and one of the cadmium peaks (277 eV) partially overlap. The surface Cd:Te atomic ratio is 1.09:1.0, near the stoichiometric value expected based on the hydrogen heat treatment literature[116].

Table 5-1. Auger Parameters of Six Elements

Element	Transition	Maximum Peak Position (eV)	Relative Sensitivity Factor	Surface Atomic Fraction, Figure 5-1
Cd	MNN	376	1.0	48.2%
Te	MNN	483	0.45	43.1%
O	KLL	510	0.5	3%
S	LVV	152	0.8	5.7%
Si	LVV	92	0.35	-
C	KLL	272	0.2	-

In general, gas dosing was performed when the temperature of CdTe was cooled to between -100 to -140°C. The hydrocarbon gas was directed towards the surface of CdTe by means of a collimated doser from a 20×10^{-3} Torr reservoir for 4 to 400 second, representing effective doses of 21 - 2160 Langmuirs (L). Because of the potential for preferential evaporation of Cd at high temperature, especially in an ultra high vacuum surrounding, heating during TPD was restricted to a maximum temperature of about 680K.

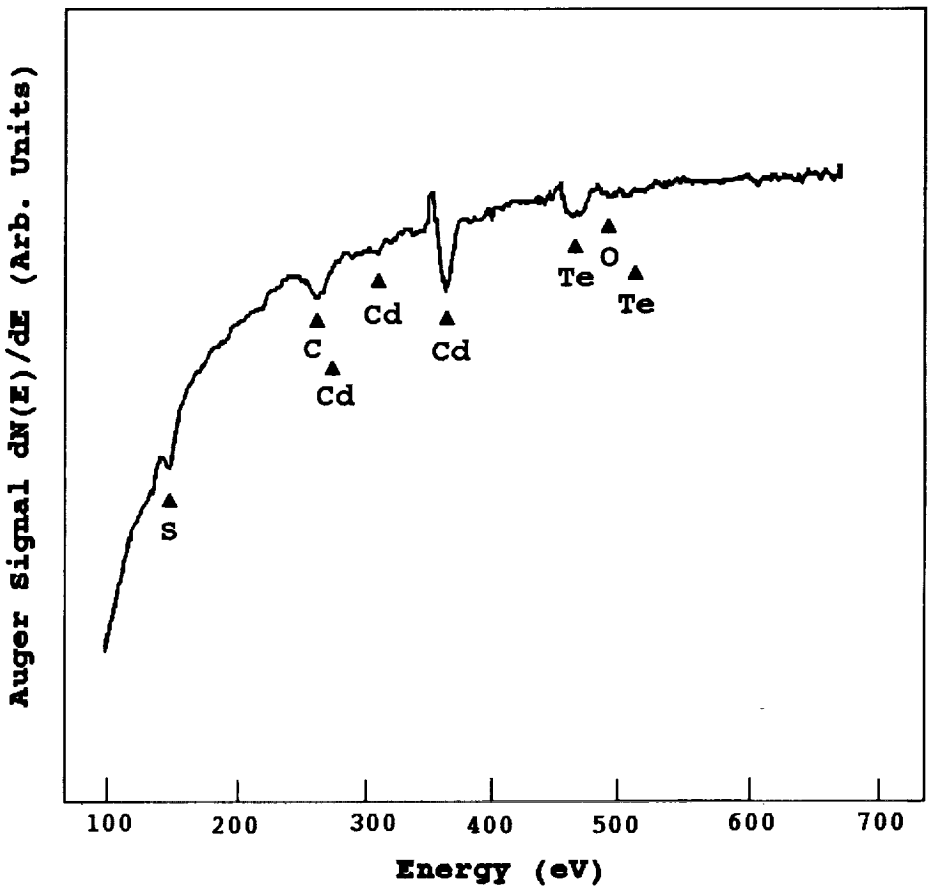

Figure 5-1 Auger Spectrum of Cleaned CdTe Surface

(V_p= 2950 V, I_B= 6 mA, V_{mod}= 6eV, t_c= 100ms, S= 3mV)

Ethylene-CdTe

Figure 5-2 represents a series of ethylene (C_2H_4) desorption traces from CdTe with varying initial coverage. Ethylene desorbs as a single, broad asymmetric peak centered at about 260K. The desorption peak temperature (T_p) is shifted by ~ 20K toward higher temperature with increasing initial coverage. If desorption is from molecularly adsorbed ethylene, and essentially follows first order kinetics, then there are two possible explanations for the observed desorption peak temperature shift. A molecularly adsorbed species with coverage dependent, attractive interactions between adsorbed molecules will exhibit upward peak shifts with increasing surface coverage. The asymmetric peak shape, with the rise below the peak maximum sharper than the tail below the maximum, is not consistent with attractive interaction. A more probable explanation is that there exists a number of similar adsorption sites which possess a range of adsorption bonding strengths.

For both linear and hyperbolic heating functions, there exists an almost linear relationship between the first order desorption peak temperature T_P and the desorption activation energy E_d. Redhead showed that for first order desorption the activation energy of desorption is approximately related to the temperature T_P though the expression :

$$E_d = R\,T_p\,[\,\mathrm{Ln}\,(\frac{\nu\,T_p}{\beta})\,-\,3.46\,]$$

where $\beta = dT/dt$ is the heating rate.

The accuracy of this method hinges on the specification of the pre-exponential factor ν. In the literature, the pre-exponential factor for first order desorption is usually assumed to be 10^{13} sec^{-1} as predicted from transition state theory (TST). Using this value, the average activation energy for ethylene desorption from CdTe is estimated to be about 67 kJ/mole at 270K. This value is consistent with that found for weakly chemisorbed gases, which usually exhibit first order desorption. Table 5-2 compares the desorption activation energy calculated from the Rough Estimate and the Desorption Peak Temperature Method.

Recently, Clemen et al.[118] studied the thermal desorption behavior of ethylene on Si(100). Their results showed that ethylene desorbed thermally from the Si surface without decomposing. The measured desorption activation energy at low coverage was 38.0 ± 1.5 kcal/mol and a pre-

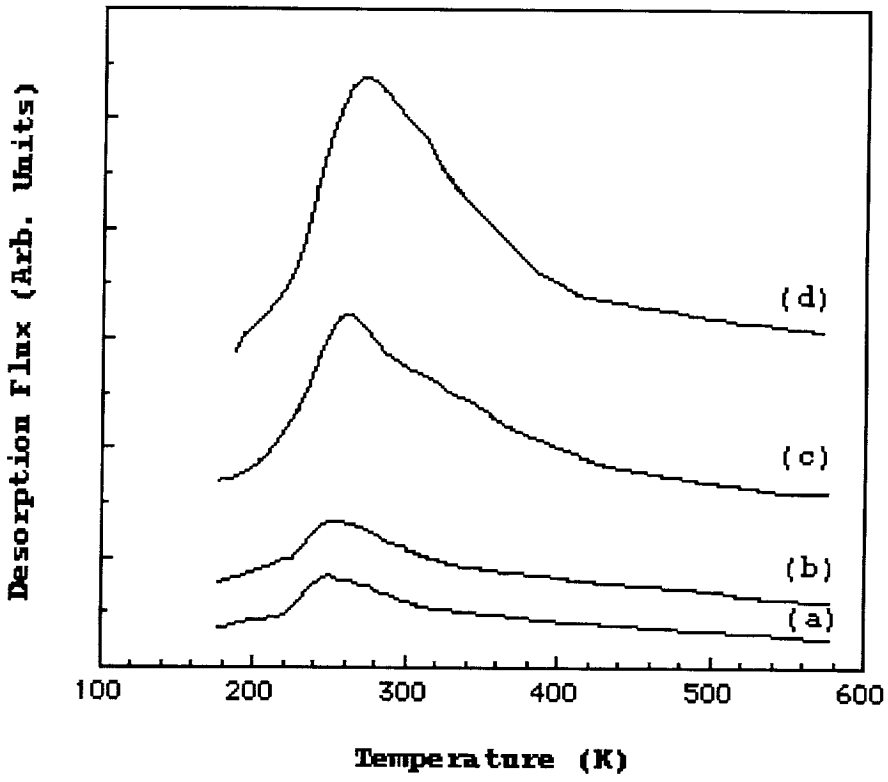

Figure 5-2 TPD Spectra of Ethylene from CdTe. Following (a)810L, (b)1,080L, (c)1,620L, and (d)2,160L exposure of ethylene at ~ 160K.

exponential factor of $\nu = 5 \times 10^{13 \pm 0.5}\ s^{-1}$. Variation of E_d with coverage suggested that attractive forces might occur between adsorbed C_2H_4 molecules on the Si(100) surface.

Table 5-2. Desorption Activation Energies of Ethylene from CdTe

T_p (K)	Rough Estimate Method E_d (kJ/mol)	Desorption Peak Temperature Method E_d (kJ/mol)
245	64	61
250	65	62
260	68	65
270	71	67

The cracking patterns published[119] for methane, ethane and ethylene are shown in Table 5-3. The desorption curves for the various cracking fragments (e.g., 27 and 26 amu) for ethylene (28 amu) are all consistent with the expected cracking pattern, further supporting the conclusion that ethylene does not decompose upon interaction with the CdTe surface.

Table 5-3. Cracking Pattern of Methane, Ethane and Ethylene

Methane (CH_4)			Ethane (C_2H_6)			Ethylene (C_2H_4)		
16	15	14	28	27	30	28	27	26
100%	85%	16%	100%	33%	26%	100%	63%	61%

Ethane-CdTe

The temperature programmed desorption spectra of ethane from CdTe (111)A, shown in Figure 5-3, are characterized by a single desorption peak with a symmetric peak shape. Table 5-4 summarizes the TPD peak temperatures exposures and relative coverages for the spectra of Figure 5-3. The desorption peak temperature shifts from 278 K to 224 K with increasing initial ethane coverage. This behavior, along with the symmetrical shape of the peak, are normally indicative (but

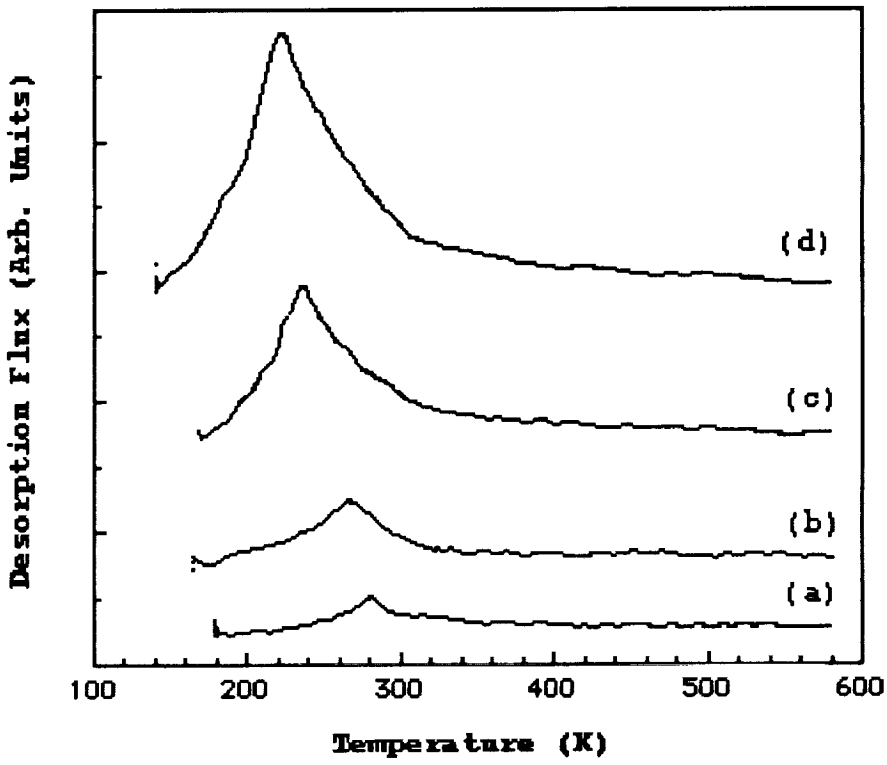

Figure 5-3 TPD Spectra of Ethane from CdTe. Following (a)22L, (b)55L, (c)440L, and (d)550L exposure of ethane at ~ 160K.

not necessarily unique) of second-order desorption kinetics[120].

Table 5-4. TPD Data Summary for Ethane from CdTe

Curve	Exposure (Langmuir)	Relative Fractional coverage	T_p (K)
1	22	0.29	278
2	55	0.36	260
3	440	0.82	236
4	550	1	224

The desorption activation energy was estimated from Redhead's equation

$$\left(\frac{E_d}{R\,T_p^2}\right) = \left(\frac{\nu_2\,\theta_0}{\beta}\right) \exp\left(-\frac{E_d}{R\,T_p}\right)$$

for second order desorption kinetics. The value of θ_o can be found from the area under the desorption curves. An Arrhenius plot of ln ($\theta_0 T_P^2$) versus $1/T_P$ values for different initial coverage yields a straight line with a slope equal to the positive desorption activation energy E_d over R, as shown in Figure 5-4. For a heating rate equal to 8 K/s, a desorption activation energy of 10.1 $\pm$ 0.5 kJ/mole and ν_2 equal to 17 cm^2/s are obtained. The calculated sticking coefficient for adsorption is estimated to be $6x10^{-3}$ from the fractional coverage *vs.* exposure data plotted in Figure 5-5. The surprisingly low value for E_d suggests that the dissociated hydrocarbon fragments on CdTe readily re-associate prior to desorption. The decreasing variation in T_p with coverage might have an alternative explanation. If ethane adsorbs molecularly on CdTe (111)A, the peak temperature shift would be indicative of repulsive forces between adjacent adsorbate molecules.

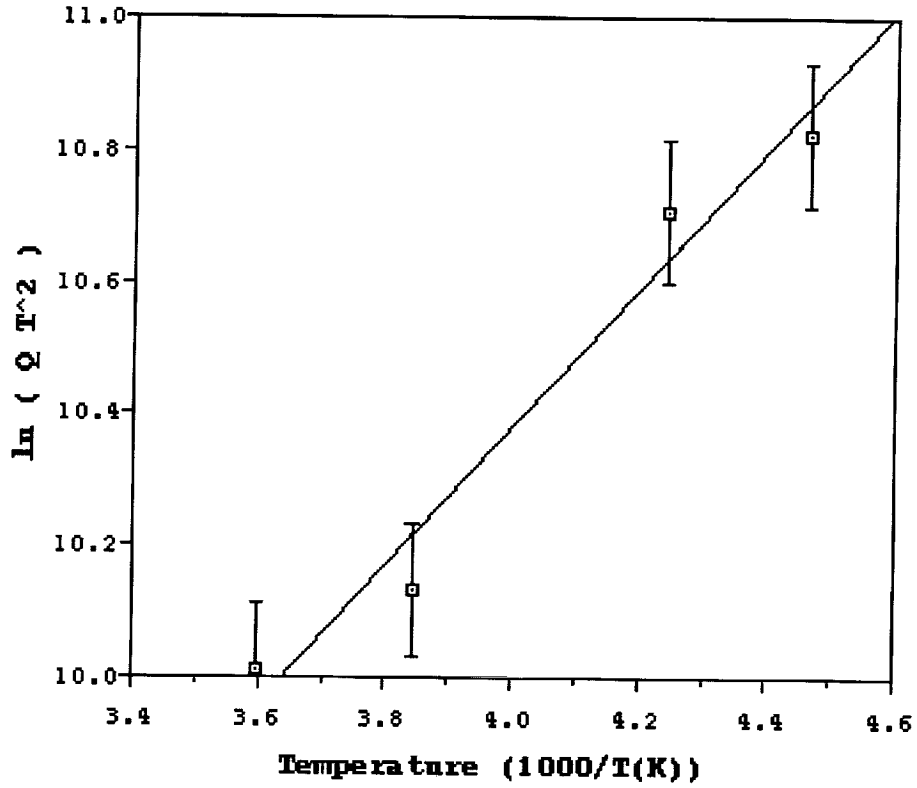

Figure 5-4 ln (θ T_p^2) *vs.* $1/T_p$ for the data of figure 5-3. 1% of the Y-axis coordinate is used as the error bar and the fitting equation is ln (θ T_p^2) = 6.184 + 1048.8($1/T_p$).

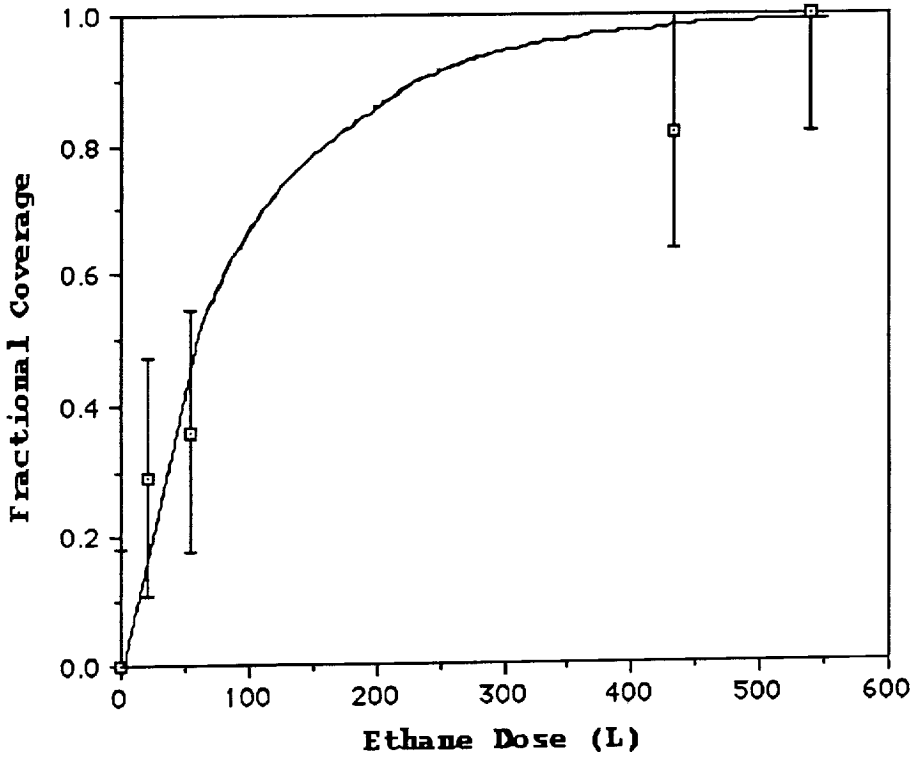

Figure 5-5 Fractional coverage *vs.* ethane exposure at 160K. The curve is the sticking coefficient of ethane on CdTe(111). Sticking coefficient at zero coverage is equal to 0.006

Methane-CdTe

Temperature programmed desorption experiments showed that methane does not adsorb on CdTe even during exposure at temperatures as low as 120K.

ii. Desorption of DETe from CdTe and Si

DETe-Si

The results for diethyltelluride (DETe) desorption from CdTe and Si are presented in this section. The cleaning procedures for CdTe are the same as described in the first section. Silicon samples were prepared from silicon (100) wafers with p-type bulk doping (ρ=1~10 Ω-cm). Before loading the Si sample into the UHV chamber, chemical etching steps were employed to remove contaminants and to form a well-defined thin oxide layer. After transferring the sample into the UHV chamber the oxide layer was removed by heating the sample in UHV to temperatures between 800°C and 900°C for 2 minutes. The cleaned Si surface was analyzed by Auger electron spectroscopy (AES). Figure 5-6 shows an Auger spectrum of the silicon surface with peaks indicating the presence of silicon (92 eV) with a trace of carbon (272 eV). The surface is essentially free of oxygen (510 eV). The total impurity is less than 3 atomic %.

Three dominant high mass peaks appear in the mass spectrum of DETe at 188, 159 and 130 amu, corresponding to the species $(C_2H_5)_2Te^+$, $(C_2H_5)Te^+$ and Te^+. The published cracking pattern of DETe[121] is shown in Table 5-5.

Table 5-5. Cracking Pattern of DETe

27	29	130	159	188
$C_2H_3^+$	$C_2H_5^+$	Te^+	$C_2H_5Te^+$	$(C_2H_5)_2Te^+$
32%	33%	75%	35%	100%

In the TPD studies all possible cracking products were tracked during the temperature ramp. The desorption flux spectra shown correspond to those for the parent ion $(C_2H_5)_2Te^+$. Unless otherwise noted, the flux spectra for the

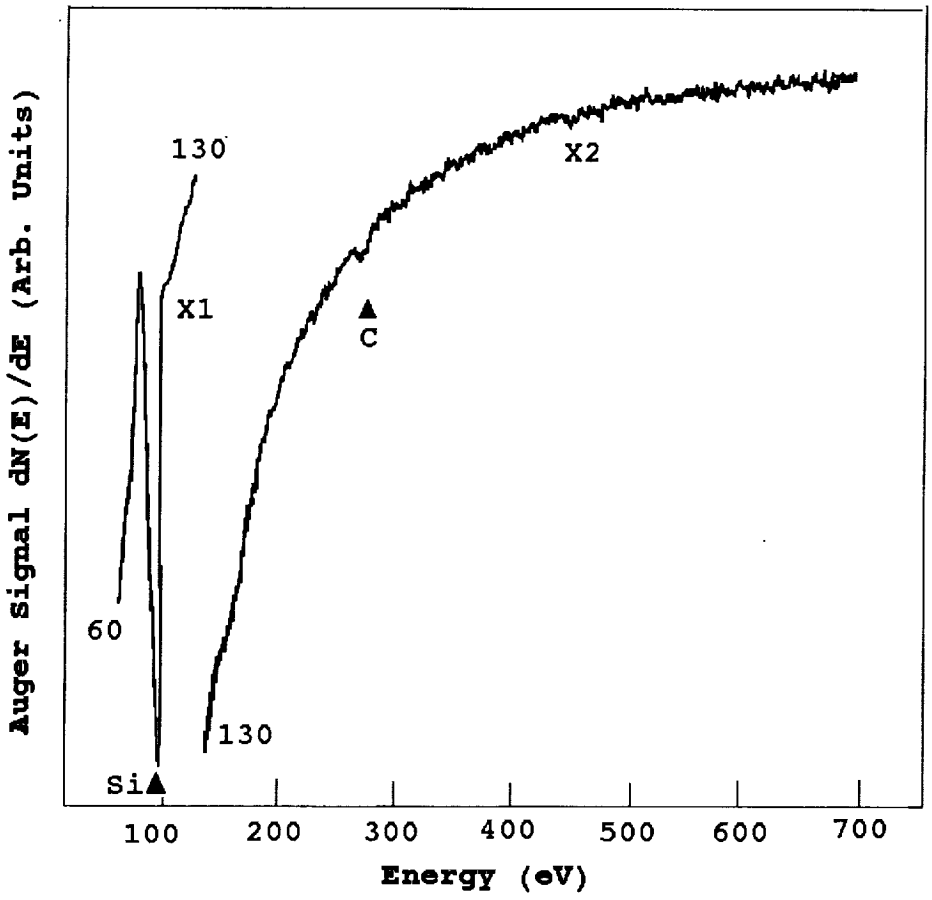

Figure 5-6 Auger Spectrum of Cleaned Si Surface

(V_p= 2950 V, I_B= 6 mA, V_{mod}= 6eV, t_c= 100ms, S= 3mV)

lower mass ions were identical in shape and position to those for the parent ion.

Figure 5-7 shows the low temperature region of a series of TPD spectra taken during DETe desorption from silicon. The inset shows the entire TPD spectra up to 600K. In these experiments the heating rate was 15 K/s, and the doses varied from 4,300 L to 15,600 L. The single intense desorption peaks exhibit two distinct features. First, the asymmetric shape of the experimental TPD curves suggests a first order desorption process, indicative of molecular adsorption and desorption. Second, DETe desorption peaks shift downward in temperature with increasing exposure, showing that the adsorption strength (desorption activation energy) is a function of surface coverage.

For first order desorption kinetics, the observed shift of the desorption peak maximum to lower temperature can be simulated by decreasing E_d or increasing the pre-exponential factor as the coverage increases[122]. Assuming a constant desorption pre-exponential factor of 10^{13}/s, we estimate a low coverage desorption activation energy of ~ 43 kJ/mole at 177 K. Table 5-6 shows estimated desorption activation energies; the relatively low values are consistent with a physisorption mechanism. Decreasing desorption energies with increasing coverage suggest the presence of repulsive interactions in the adsorbed layer.

Figure 5-8 shows TPD spectra of four cracking fragments, 29, 130, 159 and 188 amu in a single TPD experiment. Because the TPD spectra of all cracking products of DETe from Si substrate exhibit the same positions and peak temperatures as those for the parent ion, it is believed that DETe does not decompose on the Si substrate during the

Table 5-6. Desorption Activation Energies of DETe from Si

T_p (K)	Rough Estimate Method E_d (kJ/mol)	Desorption Peak Temperature Method E_d (kJ/mol)
177	46	43
175	46	42
169	44	41
161	42	39

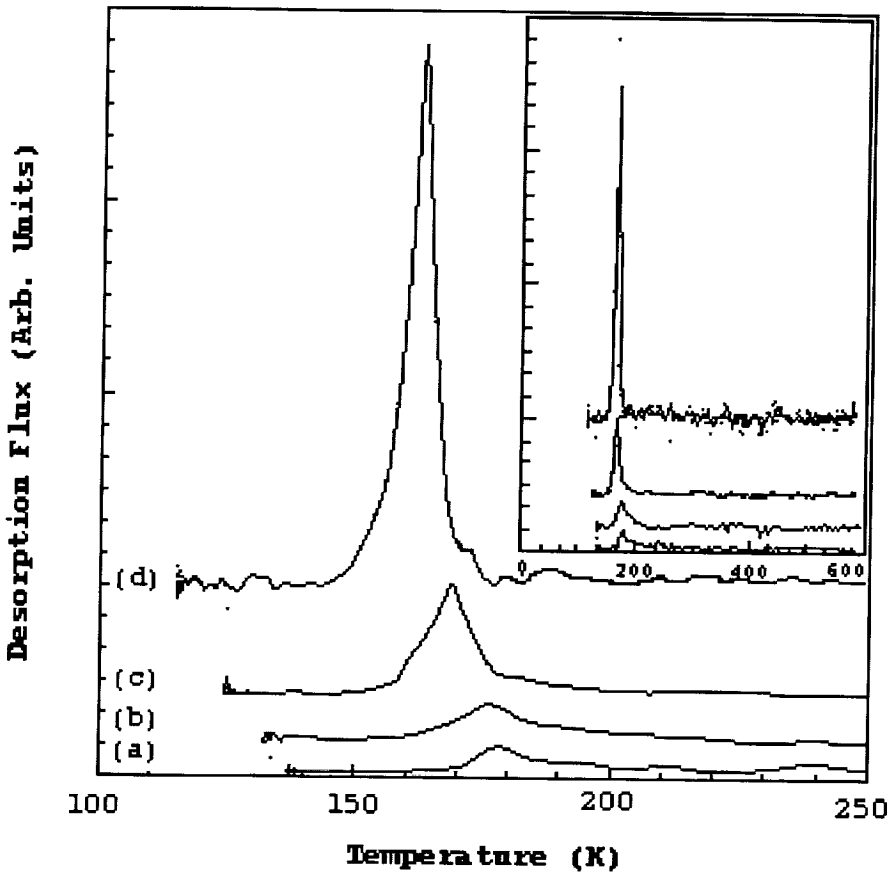

Figure 5-7 TPD Spectra of DETe from Silicon (100). Following (a)4,300L,(b)6,500L,(c)9,100L,and(d)15,600L exposure of DETe at ~ 160K.

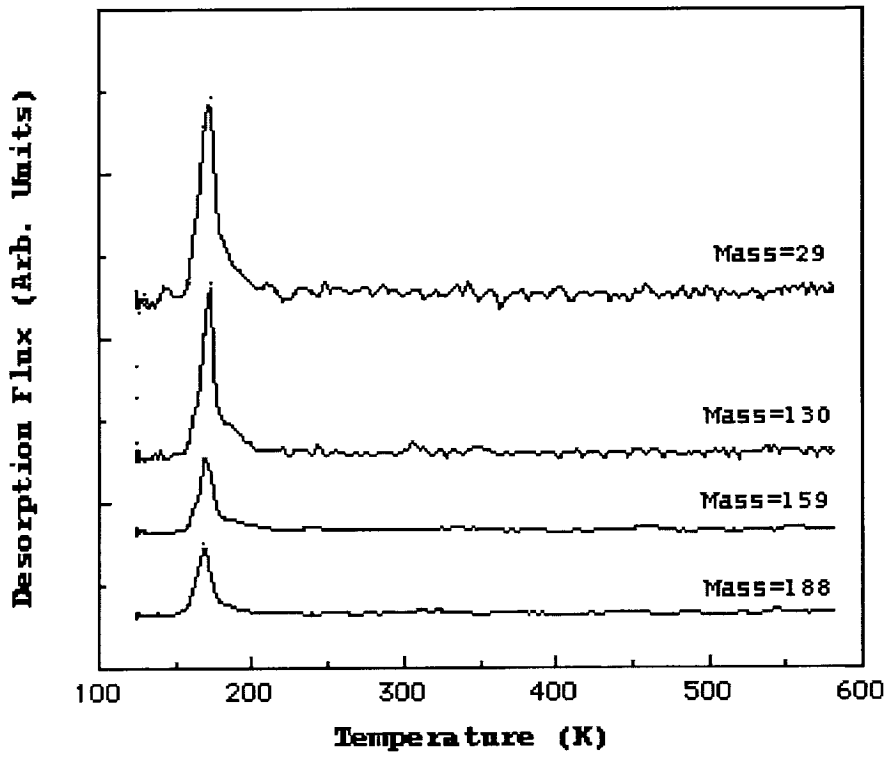

Figure 5-8 The four principal cracking fragments of diethyltelluride (188 amu,159 amu,130 amu and 29 amu) followimg 9,100L diethyltelluride exposure at ~ 140K.

temperature ramp. No Te could be detected on the Si surface using AES following the TPD experiments, in further support of this conclusion.

DETe-CdTe

The TPD spectra of DETe from the CdTe (111)A surface shown in Figure 5-9 contain two distinct desorption peak maxima, a narrow, intense peak at approximately 260 K and a broad, less intense peak centered at about 410 K. The shape of the low temperature desorption peak and the nearly invariant peak temperature are characteristic of first order kinetics, suggesting desorption of a physisorbed DETe layer or a weakly chemisorbed species. For a first order process with $\nu_1 = 10^{13}/s$ and $\beta = 9$ K/s, the desorption activation energy is on the order of 66 kJ/mole. Estimated values of E_d are summarized in Table 5-7.

The high temperature desorption peak maxima are extremely board, suggesting that a distribution of adsorption sites for strong chemisorption exist on the CdTe surface. The desorption peak temperature is centered at approximately 410K. The relative invariance of the peak temperature with varying initial coverage indicates the presence of a first order desorption process. Assuming a single molecularly adsorbed state and $\nu = 10^{13}$ s^{-1}, the estimated value of E_d for the high temperature state is approximately 107 kJ/mole.

Table 5-7. Desorption Activation Energies of DETe from CdTe

T_p (K) (1st/2nd)	Rough Estimate Method E_d (kJ/mol)	Desorption Peak Temperature Method E_d (kJ/mol)
258/405	68/106	64/102
266/410	70/107	66/103
270/415	71/109	67/105
275/427	72/112	68/108

Figure 5-10 shows three AES spectra of CdTe recorded at different stages during a TPD experiment. Curve I shows the AES spectrum of a cleaned CdTe sample; the Cd:Te surface atomic composition ratio is about 1:0.9. Curve II shows the

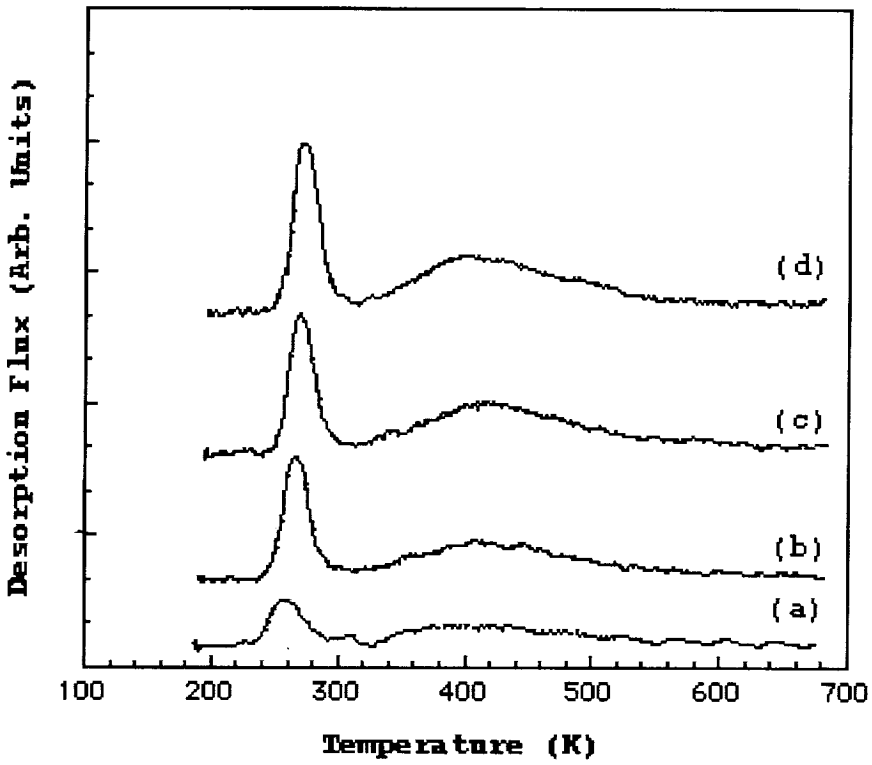

Figure 5-9 TPD Spectra of DETe from CdTe (111) following (a)10,400L, (b)14,300L, (c)18,200L, and (d)23,400L exposure of diethyltelluride at ~ 180K.

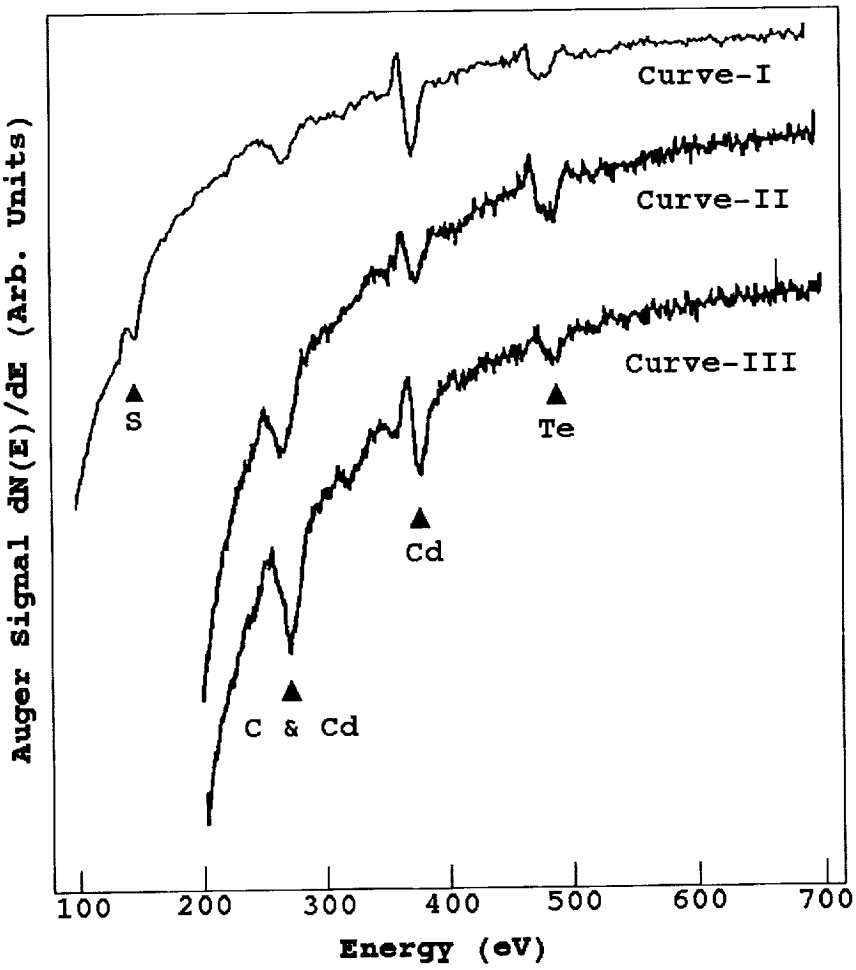

Figure 5-10 AES Spectra of CdTe (111)A surface. Curve I is for a clean surface, curve II is for after dosing and curve III is for after TPD experiment. (V_p= 2950 V, I_B= 6 mA, V_{mod}= 6eV, t_c= 100ms, S= 3mV).

AES spectrum of CdTe after dosing DETe at low temperature; the Cd:Te ratio decreased to ~ 1:3 reflecting the presence of adsorbed DETe. Curve III shows the AES spectra after the TPD experiment in which the crystal was flashed to nearly 700K. Following this thermal treatment, the surface ratio of Cd:Te became 1:0.83. It appears that the surface may have become slightly enriched in Cd during the flash. Because of the interference between the C and Cd peaks near 270 eV, it is difficult to determine whether or not C is deposited on the surface. Figure 5-11 shows TPD spectra of four cracking mass-to charge ratios, 188, 159, 130 and 29 amu, for a single TPD experiment. The curves have the same peak positions and shapes. The relative intensities area under the peaks of the two desorption peaks are in the ratio 6:7:18:20 for the 188, 159, 130 and 29 amu ions, compared to the published cracking pattern[7] of 100:35:75:33. The failure to achieve an exact match between the measured and published patterns is not unexpected since the relative sensitivity factors for each cracking fragment are a function of ionization efficiency of the gas, the transmission factor of the quadrupole filter, and the relative gain used in the multiplier mode. The 6:7:18:20 measured ratio is in good agreement with the ratio measured for thermal desorption of DETe from Si (as 6:7:15:16 in Figure 5-8). Based on the data in Figure 5-10 and Figure 5-11, it is believed that DETe does not decompose on the CdTe substrate.

iii. Desorption of DMCd from CdTe and Si

DMCd-Si

The results for DMCd desorption from Si are presented in this section. The cracking pattern of DMCd[123] is shown in Table 5-8. In general, all of these ions were tracked during the TPD experiments. Typically only the amu 129 data are reported except as noted.

Table 5-8. Cracking Pattern of DMCd

14	15	16	27	114	128	129	144
CH_2^+	CH_3^+	CH_4^+	$C_2H_3^+$	Cd^+	CH_2Cd^+	CH_3Cd^+	$(CH_3)_2Cd^+$
1,1%	3.63%	2.32%	1.43%	91.2%	9.65%	100%	35.8%

TPD spectra in Figure 5-12 collected after dosing DMCd at 180 K show a single, sharp low temperature desorption

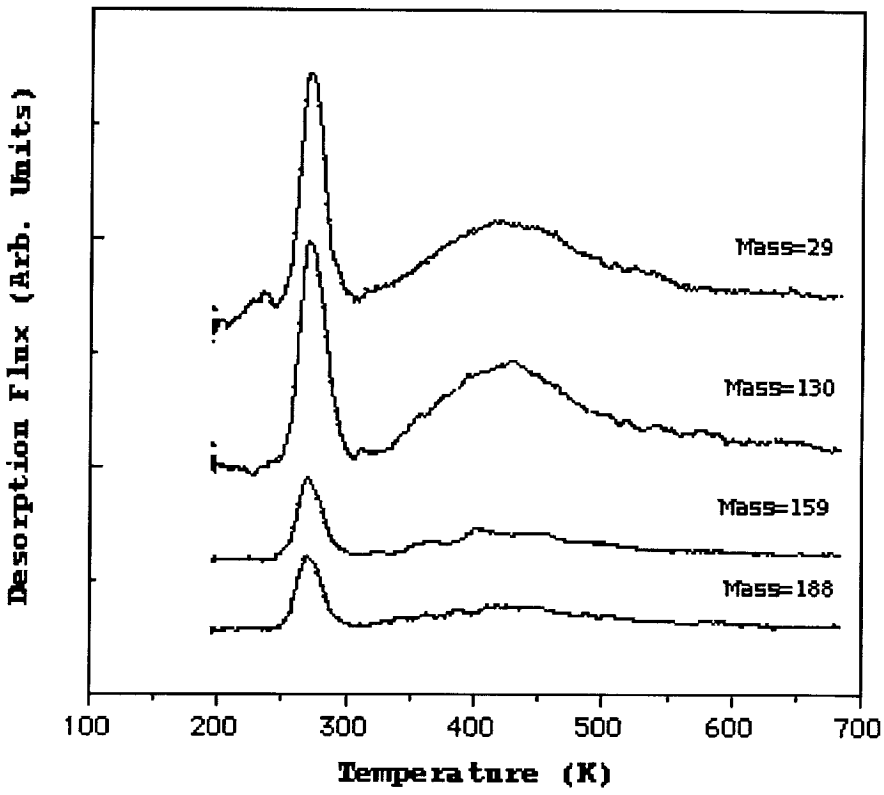

Figure 5-11 The four principal cracking fragments of diethyltelluride (188 amu,159 amu,130 amu and 29 amu) following 18,200L diethyltelluride exposured at ~ 180K from CdTe.

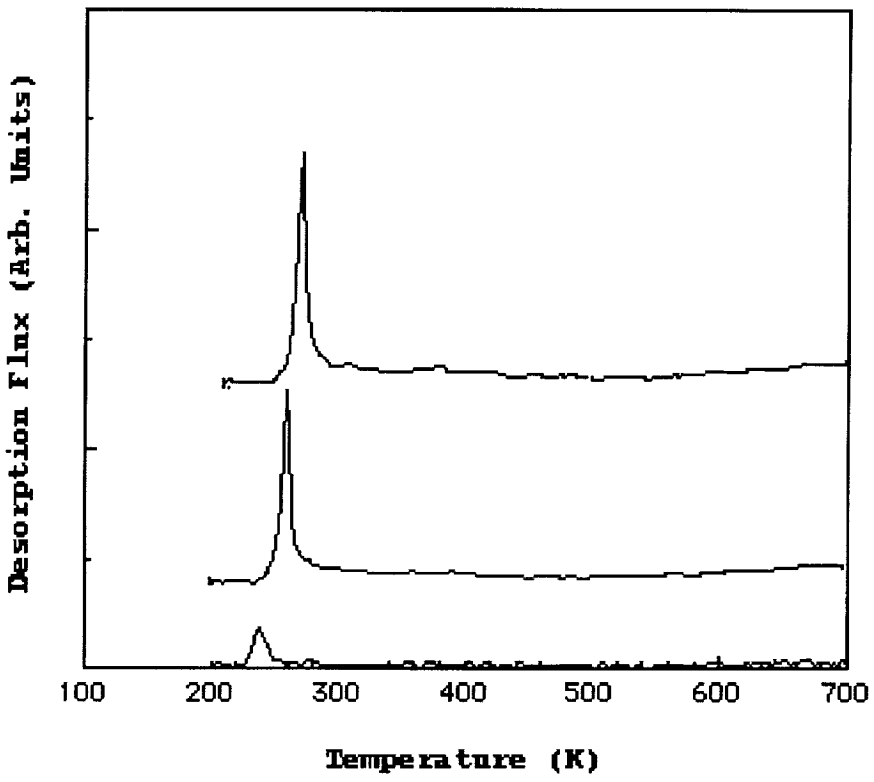

Figure 5-12 TPD Spectra of DMCd from Silicon (111) following (a)3,900L, (b)9,100L, and (c)11,700L exposure of dimethylcadmium at ~ 190K.

peak. The shapes of the experimental TPD spectra indicate the presence of a first order desorption process. Unlike DETe, the desorption peak maxima shift to higher temperature with increasing coverage. In addition, the desorption peak temperature of DMCd from Si is higher than that of DETe from Si for nearly equal heating rates, suggesting a stronger interaction with the Si surface. Figure 5-13 shows the seven cracking fragments of DMCd, 14, 15, 16, 27, 114, 129, and 144 amu from a single TPD experiment.

For a heating rate of 17 K/s and a first order pre-exponential factor of 10^{13} s^{-1}, the low coverage desorption activation energy for DMCd from Si is ~ 60 kJ/mole. The activation energies of DMCd from Si at different initial coverages are summarized in Table 5-9.

Table 5-9. Desorption Activation Energies of DMCd from Si

T_p (K)	Rough Estimate Method E_d (kJ/mol)	Desorption Peak Temperature Method E_d (kJ/mol)
235	62	57
260	68	63
270	71	73

Theoretical treatments of the thermal desorption of adsorbates have shown that adsorbate-adsorbate interactions may be the source of the observed coverage dependence for the activation energy for desorption[124]. Assuming the presence of pairwise interactions[125] and a constant pre-exponential factor ν , the desorption activation energy E_d follows the form,

$$E(\theta) = E_0 - w\theta$$

where $E_0 = E\ (\theta = 0)$ or the zero coverage energy, w is the interaction energy (positive value for repulsive, and negative for attractive), and θ is fractional surface coverage. Attractive interactions will shift the desorption peak to higher temperature, whereas repulsive interactions

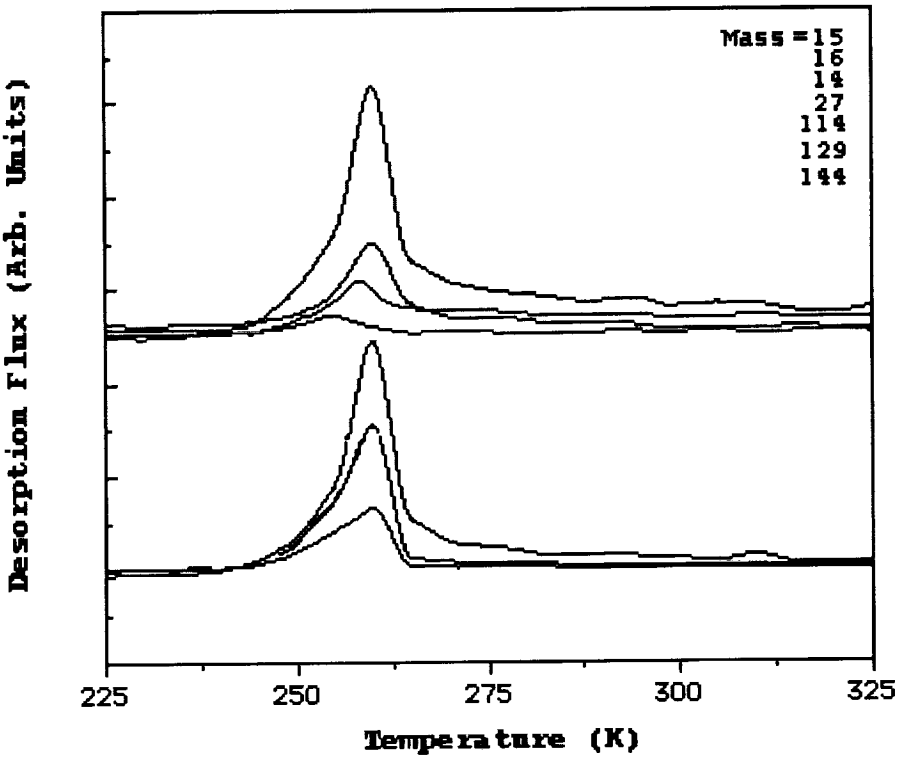

Figure 5-13 Seven Cracking Fragments, 144 amu, 129 amu, 112 amu, 27 amu, 14 amu, 16 amu and 15 amu following 9,100L DMCd exposure at ~ 180K.

shift the peaks to lower temperature. If adlayer interactions are responsible for observed peak temperature shifts with coverage, then one can conclude that DETe molecules have repulsive interactions and DMCd molecules experience attractive interactions on the Si surface.

DMCd-CdTe

TPD spectra in Figure 5-14 show three distinct desorption features as follows: (i) a low temperature sharp desorption peak at about 320 K, and (ii) a broad desorption peak at about 460 K overlapping with (iii) another high temperature peak at ~ 540 K. The asymmetric shapes of the peaks and the relative invariance of the peak temperatures with coverage indicate the presence of first order kinetics. The low temperature desorption peak shifts to higher temperature with increasing coverage. Both the high temperature states and the low temperature states, desorb at higher temperatures than the corresponding DETe states on CdTe, suggesting that there are stronger interactions between DMCd molecules and the CdTe surface than between DETe molecules and the CdTe surface. DMCd and DETe molecules both have attractive interactions on CdTe surface. Estimated desorption activation energies for DMCd from CdTe are shown in Table 5-10.

Table 5-10. Desorption Activation Energies of DMCd from CdTe

T_p (K)	Rough Estimate Method E_d (kJ/mol)	Desorption Peak Temperature Method E_d (kJ/mol)
300/440/525	79/115/138	74/110/133
320/450/530	84/118/139	80/113/134
327/460/535	86/120/140	81/116/135
335/465/540	88/122/141	83/117/136

Figure 5-15 shows two AES spectra of CdTe recorded at different stages during a TPD experiment. Curve I indicates

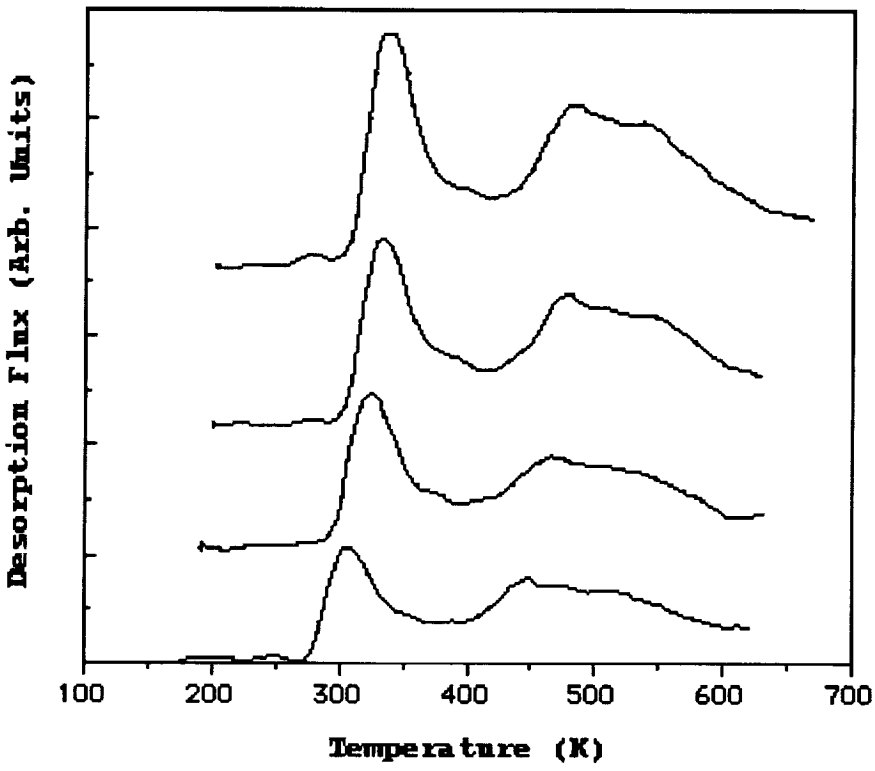

Figure 5-14 TPD Spectra of DMCd from CdTe(111) following (a)10,400L, (b)14,300L, (c)18,200L, and (d)22,000L exposure of DMCd at ~ 160K.

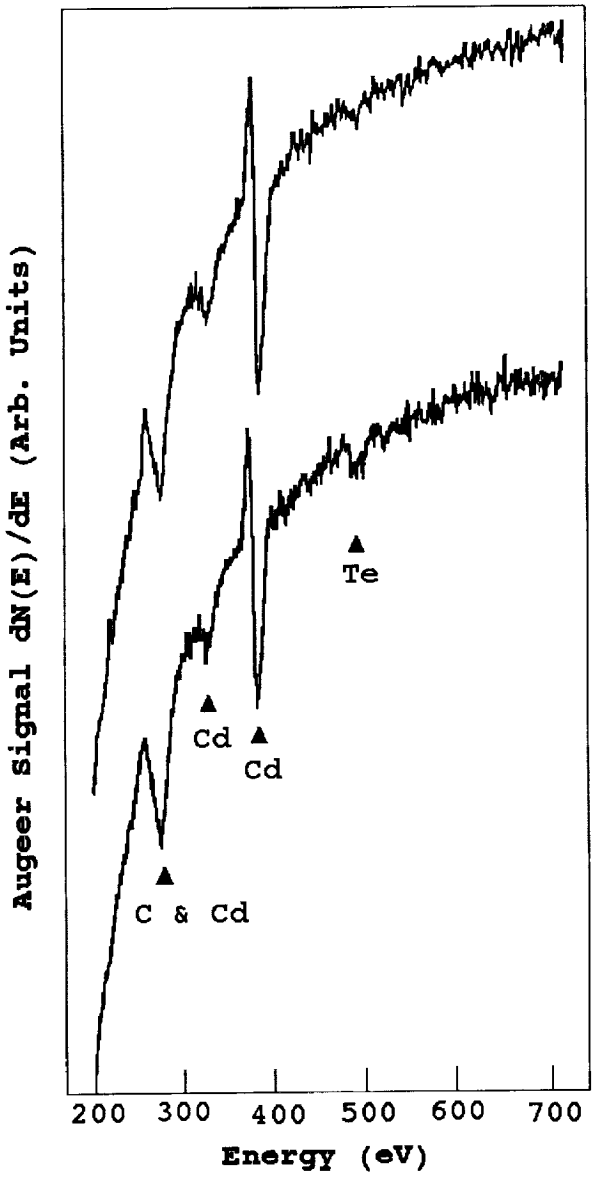

Figure 5-15 AES Spectra of DMCd on CdTe. Curve I was obtained after dosing and curve II was obtained after the TPD flash.(V_p= 2950 V, I_B= 6 mA, V_{mod}= 6eV, t_C= 100ms, S= 3mV)

that the composition ratio of Cd to Te is 5/1 after the CdTe substrate is dosed with DMCd at low temperature, compared to the 1.1:1 ratio prior to dosing, reflecting adsorption of DMCd. Curve II shows that the composition ratio of Cd to Te decreased to 2.6/1 after the CdTe substrate was subsequently heated to 620 K. Figure 5-16 shown that seven cracking masses of DMCd, 14, 15, 16, 27, 114, 129 and 144 , from TPD experiments. The peak positions and shapes of the various fragments are essentially identical. The greater intensity of the 114 amu peak suggest that Cd is deposited at low temperature, and then desorbs upon heating. Bhat et. al[62] found that DMCd decomposed between 230 and 360^{0}C. On the basis of the AES and TPD spectra, it is believed that a fraction of the adsorbed DMCd has decomposed on the CdTe substrate.

B. Discussion

i. Summary of TPD Results

Table 5-11 show summarizes the TPD experiments on CdTe and Si. The initial sticking factors for ethylene and ethane on CdTe are higher than these for DMCd and DETe on CdTe. Ethylene is molecularly adsorbed and exhibits attractive interaction on CdTe. Ethane may be dissociatively adsorbed on CdTe, perhaps forming methyl ligands at Cd surface sites. The desorption curves of metalorganic gases from CdTe and Si suggested that the source gases interacted only weakly withSi surfaces, but significantly more strongly with CdTe. The desorption activation energies of both DETe and DMCd from Si are indicative of physisorption or weak chemisorption. These results suggested that homogeneous decomposition reactions may be required to nucleate CdTe on Si substrates in MOVPE. DMCd interacts more strongly with CdTe (111)A than does DETe. Moreover, the experiments provide evidence that DMCd decompose on CdTe even at very low temperature, and in the absence of a carrier gas. DETe on the other hand does not decompose heterogeneously under the conditions of this study.

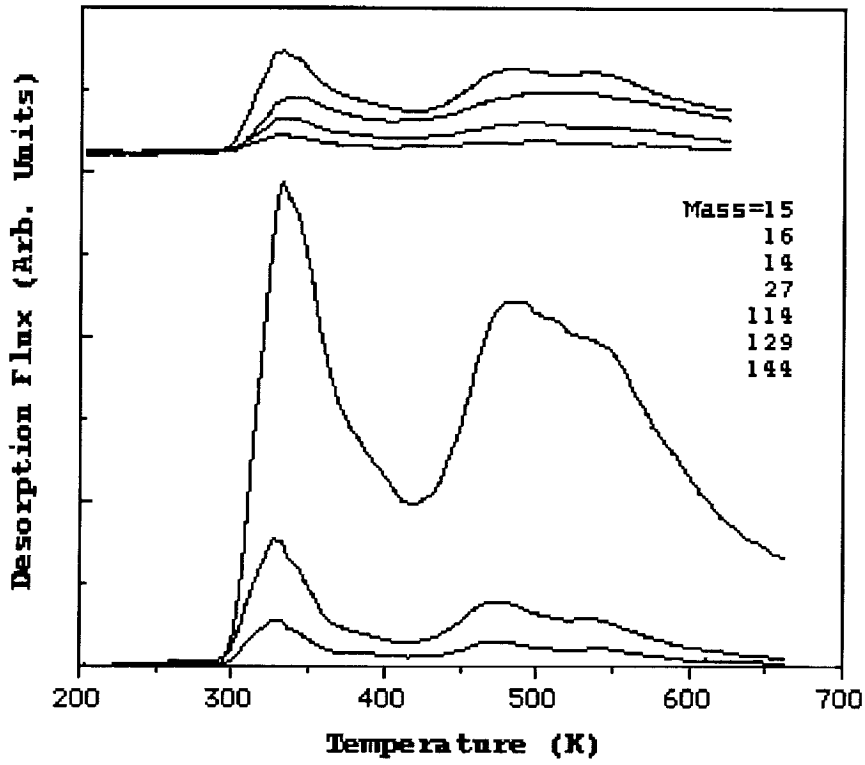

Figure 5-16 The seven principal cracking fragments of dimethylcadmium (144 amu, 129 amu, 112 amu, 27 amu, 14 amu, 16 amu and 15 amu) following 22,000L diemethylcadmium exposure at ~ 180K.

Table 5-11. Summary of TPD Experiments from CdTe and Si

Sample	Ad-sorbate	TPD Parameters	Kinetic Order	E_d (kJ/mol) (at ~ K)	Interaction between adsorbates
CdTe	C_2H_4	$20x10^{-3}$torr 150s~400s β = 8K/s	First	67 (270K)	Attractive
CdTe	C_2H_6	$20x10^{-3}$torr 4s ~ 100s β = 8K/s	Second	10 (278K)	Repulsive -
CdTe	DETe	$80x10^{-3}$torr 8~18 min β = 9K/s	First	108 (427K)	Small Attractive
CdTe	DMCd	$80x10^{-3}$torr 5~17 min β = 10K/s	First	117 (465K)	Large Attractive
Si	DETe	$80x10^{-3}$torr 200s~12 min β = 15K/s	First	43 (177K)	Repulsive
Si	DMCd	$80x10^{-3}$torr 3~9 min β = 17K/s	First	73 (270K)	Attractive

ii. Discussion of the Forces Between Adsorbates

To understand the forces between adsorbates on the substrates CdTe and Si, it is worthwhile to recall the electron configurations of cadmium (Cd), and tellurium (Te). Cadmium, an element in the group II-family, possesses a $5s^2$ valence configuration, so that it will bind at most two hydrogen atoms to form CdH_2, with a bond angle of 180 degrees. In dimethylcadmium, Cd combines with two methyl ligands to form two covalent bonds 180 degrees apart, *i.e.*, it is a linear molecule. Tellurium has a $5s^2\ 5p^4$ valence configuration. Therefore, Te will also bind two hydrogen atoms to form TeH_2, but with a bond angle of 90.6 degrees. In diethyltelluride, Te combines with two ethyl ligands to form two covalent bonds 90.6 degrees apart. The covalent bonds and two lone pairs are directed towards the vertices of a tetrahedron. When cadmium and tellurium are incorporated into the zincblende crystal structure [126], the elemental orbitals rehybridize to form an sp^3 configuration with four bonds directed towards the vertices of a tetrahedron. The atoms accomplish this by forming two covalent bonds and two dative bonds. In the dative bonds the two Te lone pairs donate to the empty p orbitals of Cd. One covalent bond extrudes from the <111> orientation. The closest distance between atoms on CdTe <111> is 4.58 Å. In contrast, for the silicon, diamond structure, there are two covalent bonds extrude from <100> orientation and the closest distance between atoms on Si<100> is 3.84 Å . Usually, the Si atoms on the <100> surface will dimerize[127] in a (2x1) or (1x2) structure.

Consider the case of simple hydrocarbons adsorbed on the CdTe (111) surface. Adjacent adsorbed hydrocarbon molecules are attracted to each other by intermolecular, or van der Waals, forces. When one molecule approaches a second, the electrons in the bonds of the first are affected by the electrons of the second, and the electrons in the two individual molecules begin to correlate their movements. However, there is a limit as to how close these forces can bring molecules together. At a certain proximity, nuclear-nuclear and electron-electron repulsion outweigh these attractive forces, and the interaction between molecules becomes repulsive. Ethylene[128,129] (C_2H_4) has a double C-C bond; there exists "π electron cloud" above and below the molecular. When two ethylene molecules are put together, attractive forces will adjust their electron configuration, and lower their total energy.

Consider the case of DMCd and DETe molecules adsorbed on CdTe (111) and Si (100). Si surfaces may bond these sources gases in a way that leads to shorter interatomic

distances between adsorbates than these on the CdTe (111)A surface. Because DETe molecules have two covalent bonds and two lone pairs, the nuclear-nuclear and electron-electron repulsive force will overcome the attractive force at small separation, otherwise they have attractive interaction. Hence DETe molecules absorbed on Si surface exhibit repulsive forces and on CdTe exhibit attractive forces. DMCd is a linear molecule, and will therefore show less repulsive forces between them, so that when adsorbed on Si and CdTe they will exhibit attractive interactions.

High metal alkyl exposures (thousands of Langmuirs) were required to achieve a significant extent of adsorption on the CdTe surface, and hence the sticking factors for the source gases on CdTe (111) are low. Although the sticking coefficients could not be quantified, this qualitative finding is consistent with the low measured initial sticking coefficients for dimethylcadmium and dimethyltellurium on GaAs (100) of 7 X 10^{-3} and 3 x 10^{-5}, respectively[130]. Liu et al. [65] extracted a sticking factor for DMCd and DETe of 1.5 x 10^{-4} from deposition rate on CdTe (100). In spite of it's low sticking probability, DMCd readily decomposes on CdTe with little or no activation barrier to produce Cd atoms. In contrast, DETe does not decompose under the conditions of our experiments. During CdTe MOVPE, it is likely that excess Cd atoms produced through heterogeneous decomposition of DMCd desorb into the gas phase, where they may participate in homogeneous reactions above the substrate surface. It appears that the decomposition of DETe is not catalyzed by a Cd-rich surface, at least in the absence of adsorbed hydrogen[131]. Snyder et al.(132) have observed a near quenching of the CdTe deposition rate on the CdTe (111)A surface in an impinging jet reactor when the carrier gas was switched from hydrogen to helium. It is reasonable to conclude that, at least on this surface, in the absence of hydrogen and in the absence of cooperative mechanisms between coadsorbed Cd and Te alkyls, the rate limiting step for MOVPE film growth is heterogeneous decomposition of adsorbed tellurium alkyl.

iii. The Role of Carrier Gas

No carrier gas is used in temperature programmed desorption experiments. Comparison of the TPD results with conventional deposition or pyrolysis experiments using hydrogen as a carrier gas suggests that DETe decomposes more readily in the presence of hydrogen. It seems that the carrier gas, especially hydrogen, might play more than a carrier function in MOVPE process. Recently, Snyder *et al.*[132] reported that hydrogen increased the growth rate in MOVPE CdTe with DETe and DMCd, but nitrogen and helium gases had little or no effect on growth rate. In addition, the

desorption curves suggested that the organic ligands of the metal alkyl precursors may bond to the substrate in the adsorption process. It is reasonable to propose that hydrogen gas may have two functions in MOVPE processes: one is that hydrogen atoms seem to speed the chain reaction in gas-phase decomposition reactions; the other is that hydrogen atoms scavenge adsorbed hydrocarbons on the substrates, so that the MOVPE growth rate is higher when hydrogen gas is used as a carrier gas.

REFERENCES

(1) A. L. Fahrenbruch and R. H. Bube, Fundamentals of Solar Cells: Photovoltaic Solar Energy Coversion, Academic Press, New York, (1983).
(2) A. E. Popa, IEEE G-MTT Int. Microwave Symp. Dig. Tech. Papers, 295, (1973).
(3) A. Ray Hilton, J. Electronics Materials, **2**, 211 (1973).
(4) K. Zano, Semiconductors and semimetals, Vol 13, Academic, New york, (1978).
(5) B. M. Kulwicki, Ph.D. Dissertation, University of Michigan, Ann Arbor, Michigan, (1963).
(6) D. de Nobel, Phillips Res. Rep., **14**, 361 (1959).
(7) M. Z. Kobayashi, Inorg. Chem., **69**, 1 (1911).
(8) M. R. Lorentz, J. Phys. Chem. Solids, **23**, 939 (1962).
(9) J. Steininger, A. J. Strauss and R. F. Brebrick, J. Electrochem. Soc., **117**, 1350 (1970).
(10) R. F. Brebrick, J. Electrochem. Soc., **118**, 2014 (1971).
(11) D. Long, Infrared Phys., 7, 169 (1967).
(12) M. A. Kinch, S. R. Borrello and A. Simmons, Infrared Phys., **17**, 1327 (1977).
(13) M. B. Reine, A. K. Sood and T. J. Tredwell, in "Semiconductors and Semimetals" Vol. 18, edited by R. K. Willardson and A. C. Beer, Academic Press, New York (1981).
(14) I. Melngailis and T. C. Harman, Appl. Phys. Lett., **13**, 180 (1968).
(15) M. R. Johnson, R. A. Chapman and J. S. Woobel, Infrared Phys., **15** , 317 (1975).
(16) G. Nimtz, B. Schlicht and R. Dornhaus, Narrow-Gap Semiconductors, Springer-Verlag, Berlin, (1983).
(17) D. Long and J. L. Schmit, in "Semiconductors and Semimetals", Vol. 5, edited by R. K. Willardson and A. C. Beer, Academic Press, New York, (1970).
(18) R. J. Camp, M. L. Hitchell, J. L. Schmit, and L. Stelzer, U.S. Patent 3 963 540, (1976).
(19) T. Tung, J. Cryst. Growth, **86**, 161 (1988).
(20) E. R. Gertner, Mat. Res. Soc. Symp., Vol. 90, 357 (1987).
(21) R. Korenstein, P. Hallock, and B. MacLeod, J. Vac. Sci. Technol., B **9(3)**, 1630 (1991).
(22) R. A. Reynolds, J. Vac. Sci. Technol., A **7(2)**, 269 (1989).
(23) N. M. Manasevit and W. I. Simpson, J. Electrochem. Soc., **118**, 644 (1971).
(24) J. B. Mullin, S. J. C. Irvine and D.J. Ashen, J. Cryst. Growth, **55**, 92 (1981).
(25) B. Y. Maa and P.D. Dapkus, Appl. Phys. Lett., **58**,1762 (1991).
(26) M. Grundmann, A. Krost and D. Bimberg, J. Cryst. Growth, **115**,150 (1991).

(27) J. M. Olsen and A. Kibbler, J. Cryst. Growth, **77**,182 (1986).
(28) J. H. Neave, B. A. Joyce, P. Dobson, and N. Norton, Appl. Phys., A **31**,1 (1983).
(29) J. Nishizawa and T. Kurabayashi, J. Electrochem. Soc., 130, 413 (1983).
(30) Y. Montel, M. P. Berthet, R. Favre, A. Hariss, J. Bouix, M. Vaille, and P. Gibart, J. Cryst. Growth, **77**, 172 (1986).
(31) C. M. Stahle, C. R. Helms, H. F. Schaake, R. L. Strong, A. Simmons, J. B. Pallix and C. H. Becker, J. Vac. Sci. Technol., **A7**, 474 (1989).
(32) J. I. Davies, G. Fan, M. J. Parrott, and J. O. Williams, J. Electron. Mater., **15**, 68 (1986).
(33) D. W. Shaw, J. Cryst. Growth, **31**, 130 (1975).
(34) G. B. Raupp and J. A. Dumesic, J. Phys. Chem., **88**, 660, (1984).
(35) G. H. Smuddle, Jr., X. D. Peng, R. Viswanathan, and P. C. Stair, J. Vac. Sci. Technol., **A9(3)**, 1885 (1991).
(36) R. Lin, T. R. Gow, A. L. Backman, L. A. Cadwell, F. Lee, and R. I. Masel, J. Vac. Sci. Technol., **B 7(4)**, 725 (1989).
(37) Metal-Organic Compounds , ed. by American Chemical Society, Washington, D.C. (1959).
(38) H. C. Kaufman, Handbook of Organometallic Compounds, D. Van Nestrand Company, Inc., Princeton, (1961).
(39) N. I. Sax, Dangerous Properties of Industrial Materials, Van Nostrand-Reinhold, New York, (1975).
(40) A. Allmark, Brit. J. Ind. Med., **5**, 177 (1948).
(41) S. J. Irvine and J. B. Mullin, J. Cryst. Growth, **55**,107 (1981).
(42) S. K. Ghandhi and I. B. Bhat, Appl. Phys. Lett., **44**, 779 (1984).
(43) W. E. Hoke, P. J. Lemonias, and R. Taczewski, Appl. Phys. Lett., **45**,1092 (1984).
(44) J. Bloem and L. J. Giling, Current Topics in Materials Science, **1**, 147, (1978).
(45) G. B. Stringfellow, Organometallic Vapor-Phase Epitaxy: Theory and Practice, Academic Press, Inc., New York (1989).
(46) J. Komeno, A. Miura and S. Ohkawa, J. Cryst. Growth, **45**,171 (1978).
(47) W. D. Johnston, Jr., J. Cryst. Growth, **39**, 117 (1977).
(48) D. H. Reep and S. K. Ghandhi, J. Electrochem. Soc., **130**, 675 (1983).
(49) D. Viechnicki and F. Schmidt, J. Cryst. Growth, **26**, 162 (1974).
(50) J. B. Mullin, S. J. C. Irvine, J. Giess and A. Royle, J. Cryst. Growth, **72**, 1 (1985).
(51) J. B. Mullin, S. J. C. Irvine and D. J. Ashen, J. Cryst. Growth, **55**,92 (1981).

(52) J. Giess, J. S. Gough, S. J. C. Irvine, J. B. Mullin and G. W. Blackmore, Mater. Res. Soc. Symp. Proc., vol. 90, 389 (1987).
(53) J. B. Mullin, A. Royle, J. Giess, J. S. Gough and S. J. C. Irvine, J. Cryst. Growth, **77**, 460 (1986).
(54) S. J. Irvine, J. Giess, J. S. Cough, G. W. Blackmore, A. Royle, J. B. Mullin, N. G. Chew and A. G. Cullis, J. Cryst. Growth, **77**, 437 (1986).
(55) K. Zanio, J. Vac. Sci. Technol., **A4**, 2106 (1986).
(56) P. Capper, C. D. Maxey, P.A. C. Whiffin, and B. C. Easton, J. Cryst. Growth, **96**, 519 (1989).
(57) C.-H. Sua, P.-K.Liao and R. F. Brebrick, J. Electron Mater., **12**, 771 (1983).
(58) J. B. Mullin, P. A. Clifton, G. J. Russell, A. W. Brinkman, and J. Woods, J. Cryst. Growth, **93**, 755 (1988).
(59) I. B. Bhat, H. Fardi, S. K. Ghandhi, and C. J. Johnson, J. Vac. Sci. Technol., A **6**, 2800 (1988).
(60) C. M. Laurie and L. H. Long, Trans. Faraday Soc., **53**, 1431 (1957).
(61) S. J. W. Price and A. F. Trotman-Dickenson, Trans. Faraday Soc., **53**, 939 (1957).
(62) I. B. Bhat, N. R. Taskar and S. K. Ghandhi, J. Electrochem. Soc., **134**, 196 (1987).
(63) D. A. Jackson, J. Cryst. Growth, **87**, 205 (1988).
(64) P. I. Kuznetsov, M. Safaev, V. V. Shermet, I. N. Odim and A. V. Novoselova, Inorg. Materials USSR, **19**, 787 (1983).
(65) B. Liu, A. H. McDaniel and R. F. Hicks, J. Cryst. Growth, **112**, 192 (1991).
(66) A. H. McDaniel, B. Liu and R. F. Hicks, J. Cryst. Growth, **124**, 676 (1992).
(67) R. F. Hicks, Proc. IEEE, **80**, 1625 (1992).
(68) J. K. Kochi, Organometallic Mechanisms and Catalysis, Academic Press, New york, (1978).
(69) K. F. Jensen and D. B. Graves, J. Electrochem. Soc., **130**, 1950 (1983).
(70) H.-T. Oh, S.-W. Kang and I.-S. Kang, J. Electrochem. Soc., **139**, 1714 (1992).
(71) J. Koreg, Surface Technology, **10**, 433 (1980).
(72) L. Apker, Ind. Eng. Chem., **40**, 846 (1948).
(73) H. Pfnur and D. Menzel, J. Chem. Phys., **79**, 2400 (1983).
(74) J. L. Falconer and J. A. Schwarz, Cata. Rev.-Sci. Eng., **25**, 141 (1983).
(75) J. Lee and R. J. Madix, Surface Sci., **143**, 626 (1984).
(76) G. B. Raupp and J. A. Dumesic, J. Catal., **97**, 85 (1986).
(77) J. P. Hobson and J. W. Earnshaw, J. Vac. Sci. Technol., **4**, 257 (1967).
(78) J. W. Earnshaw and J. P. Hobson, J. Vac. Sci. Techno., **5**, 19 (1968).

(79) M. Polanyi and E. Wigner, Z. Physik Chem., **A139**, 439 (1928).
(80) P. A. Redhead, Vacuum, **12**, 203 (1962).
(81) G. Carter, Vacuum, **12**, 245 (1962).
(82) J. L. Falconer and R. J. Madix, Surface Sci., **48**, 393 (1975).
(83) F. M. Lord and J. S. Kittleberger, Surface Sci., **43**, 173 (1974).
(84) D. Edwards,Jr., Surface Sci., **54**, 1 (1976).
(85) A. W. Czanderna, J. R. Biegen, and W. Kollen, J. Colloid Interface Sci., **34**, 406 (1970).
(86) R. Chen, Surface Sci., **43**, 657 (1974).
(87) C. M. Chan, R. Aris, and W. H. Weinberg, Appl. Surface Sci., **1**, 360 (1978).
(88) C. M. Chan and W. H. Weinberg, Appl. Surface Sci., **1**, 377 (1978).
(89) J. A. Konvalinka and J. J. F. Scholten, J. Catal., **48**, 374 (1977).
(90) D. F. Ollis and E. Ibok. J. Catal., **75**, 433 (1982).
(91) J. M. Criado, P. Malet, G. Hunuera, and V. Rives-Arnau, J. Catal., **75**, 428 (1982).
(92) R. J. Madix, Adv. Catal., **29**, 1 (1980).
(93) B. S. Meyerson, E. Ganin, D. A. Smith and T. N. Nguyen, J. Electrochem. Soc., **133**, 1232 (1986).
(94) B. S. Meyerson, Appl. Phys. Lett. **48**, 797 (1986).
(95) B. S. Meyerson, F. K. LeGoues, T. N. Nguyen, and D. L. Harame, Appl. Phys. Lett. **50**, 113 (1987).
(96) B. S. Meyerson, K. F. Uram, and F. K. LeGoues, Appl. Phys. Lett. **53**, 2555 (1988).
(97) V. Comello, Semiconductor Intl., **13**, 54 (1990).
(98) D. W. Greve and M. Racanelli, J. Vac. Sci. Technol. B, **8**, 511 (1990).
(99) D. W. Greve and M. Racanelli, Appl. Phys. Lett., in press.
(100) K. F. Jensen and D. B. Graves, J. Electrochem. Soc., **130**, 1950 (1983).
(101) D. P. Woodruff and T. A. Delchar, Modern Techniques of Surface Science, Cambridge University Press, London, (1986).
(102) C. L. Briant and R. P. Messmer, Auger Electron Spectroscopy, Academic Press, Boston, (1988)
(103) D. Briggs and M. P. Seah, Practical Surface Analysis: by Auger and X-ray photo-electron spectroscopy, Wiley, Chichester, New york, (1983)
(104) "Handbook of Auger Electron Spectroscopy", ed. by L. E. Davis, N. C. MacDonald, P. W. Palmberg, G. E. Riach, and R. E. Weber, Physical Electronics, Inc., Eden Prairie, Minnesota, 1976.
(105) W. Paul and H. Steinwedel, Naturforsch **8A** , 448 (1953).

(106) M. Mosharrafa, Industrial Research/Development, March, 24 (1970).
(107) R. E. March and R. J. Hughes, Quadrupole Storage Mass Spectrometry, A Wiley-Interscience Pub. Co., New York, (1989).
(108) P. H. Dawson, Quadrupole Mass Spectrometry and Its Applications, Elsevier Scientific Pub. Co., New York, (1976).
(109) Liquid Air Corporation, One Embarcadero Center, San Francisco, CA 94111.
(110) Spectra Gases, Incorporated, 3033 Industry Street, Oceanside, CA 92054.
(111) Morton Thiokol, Incorporated (CVD Inc.), 185 New Boston Street, Woburn, MA 01801.
(112) II-VI Incorporated, 375 Saxonburg Boulevard, Saxonburg, Pennsylvania 16056.
(113) M. Inoue, I. Teramoto, and S. Takayanagi, J. Appl. Phys., **33**, 2578 (1962).
(114) K. Nakagawa, K. Maeda, and S. Takeuchi, Appl. Phys. Lett., **34** , 574, (1979).
(115) A. J. Ricco, H. S. White and M. S. Wrighton, J. Vac. Sci. Technol., **A2**, 910 (1984).
(116) J.-P. Haring, J. G. Werthen, R. H. Bube, L. Galbrandsen, W. Jansen, and P. Luscher, J. Vac. Sci. Technol., **A1**, 1469 (1983).
(117) G. T. Hindman, Ph.D. Dissertation, Arizona State University, Tempe, Arizona (1989)
(118) L. Clemen, R. M. Wallace, P. A. Taylor, M. J. Dresser, W. J. Choyke, W. H. Weinberg and J. T. Yates, Jr., Surface Sci., **268**, 205 (1992).
(119) Cracking Pattern Calculator, VG Instruments, 32 Commerce Center, Cherry Hill Drive, Danvers, MA 01923
(120) C. M. Chan, R. Aris and W. H. Weinberg, Appl. Surface Sci., **1**, 360 (1978).
(121) "Eight Peak Index of Mass Spectra", ed. by The Royal Society of Chemistry, Unwin Brothers Ltd., Nottingham, (1983).
(122) V. P. Zhandov, Surface. Sci., **133**, 469 (1983).
(123) O. N. Druzhkov, R. F. Galiullina, T. K. Postnikova, Y. A. Andrianov and E. A. Pavlenko, Tr. Khim. Khim. Tekhnol., No.4, 134 (1974).
(124) A. Redondo, Y. Zeiri and W. A. Goddard III, J. Vac. Sci. Technol. **B2**, 550 (1984).
(125) L. D. Schmidt, Catal. Rev. Sci. Eng., **9**, 115 (1974).
(126) A. J. Strauss, Rev. Phys. Appl., **12**, 167, (1977).
(127) R. J. Hamers, R. M. Tromp and J. E. Demuth, Surface Sci., **181**, 346 (1987)
(128) "Comprehensive Organometallic Chemistry", ed. Sir Geoffrey Wilkinson FRS, Pergamon Press, Oxford, (1982).
(129) J. March, " Advanced Organic Chemistry", Wiley-Interscience Publication, New York, (1992).

(130) C. D. Stinespring and A. Freedman, Chem. Phys. Lett., **143(6)**, 584 (1988).
(131) R. F. Hicks, National Meeting of the AICHE, St. Louis, MO, November (1993).
(132) D. W. Snyder, P. J. Sides and E. I. Ko, J. Electrochem. Soc., **139**, L66 (1992).

Appendix I:

J. Vac. Sci. Technol. A 11(6), 3053 (1993)

Predicting intrawafer film thickness uniformity in an ultralow pressure chemical vapor deposition reactor

Gregory B. Raupp, Dimitris A. Levedakis, and Timothy S. Cale
Department of Chemical, Bio & Materials Engineering, Center for Solid State Electronics Research, Arizona State University, Tempe, Arizona 85287-6006

N15

(Received 17 August 1990; accepted 7 August 1993)

We present a reaction engineering analysis of a multiple wafer-in-tube ultrahigh vacuum chemical vapor deposition reactor which allows an estimate of wafer throughput for a reactor of fixed geometry and a given deposition chemistry with specified film thickness uniformity constraints. The model employs a description of ballistic transport and reaction based on the pseudosteady approximation to the Boltzmann equation in the limit of pure molecular flow. The model representation takes the form of an integral equation for the flux of each reactant or intermediate species to the wafer surfaces. Expressions for the reactive sticking coefficients (RSC) for each species must be incorporated in the term which represents reemission from a wafer surface. In our model we use a published expression for the RSC of silane as a function of flux and wafer temperature developed from molecular beam measurements. Numerical solution of the resulting integral equation using Gauss–Legendre quadrature yields quantitative estimates of intrawafer film thickness uniformities for epitaxial silicon deposition from silane for specified process conditions and wafer radius:wafer separation. For given reactor dimensions and specified uniformity, throughputs can then be estimated.

I. INTRODUCTION

Meyerson and co-workers have experimentally demonstrated dramatic advantages to reduced temperature, ultralow pressure ($P \leqslant 0.001$ Torr) operation in chemical vapor deposition (CVD) of epitaxial silicon.[1–3] Silicon films deposited at ultralow pressures are essentially defect free and are of high purity.[1,2] Dopants can be incorporated to levels well above their solid solubility limits, and because of the relatively low deposition temperatures, junctions are abrupt.[3] Heteroepitaxial films and superlattice structures of SiGe are readily deposited.[4] An ultrafast (75 GHz) heterojunction bipolar transistor (HBT) has been fabricated using this technology to grow a boron-doped SiGe base region.[5]

To realize these advantages, the reduced temperature and pressure process is performed in a custom designed ultrahigh vacuum reactor; for this reason Meyerson has called the process ultrahigh vacuum chemical vapor deposition (UHV/CVD). The clean environment allows surface silicon oxide and hydride contaminant layers to be removed *in situ* by a high temperature bake in vacuum prior to deposition.[1,2] The resulting oxide-free surface provides a high quality surface on which epitaxial silicon deposits from silane containing gas mixtures at temperatures significantly lower than conventional low pressure, cold wall epitaxial deposition processes (1023–1123 K versus 1273 K or greater). Growth of SiGe layers can be accomplished at even lower temperatures.[4,6,7] Deposition itself is carried out at a total pressure on the order of 10^{-3} Torr. Since these pressure levels are significantly lower than those conventionally employed in low pressure CVD reactors, we prefer to call processing of this type ultralow pressure chemical vapor deposition (ULPCVD), and will use this terminology interchangeably with UHV/CVD.

Although the use of reduced temperatures and pressures during deposition enhances material and device properties, throughput may be an issue in a production environment since these conditions also lead to significantly reduced deposition rates. Low throughput may be mitigated by employing load-locked wafer handling and a volume-loaded multiple wafer-in-tube hot wall reaction chamber.[1,2,6] To maximize throughput in such a reactor, wafer spacing and reaction conditions must be chosen to maximize deposition rate while meeting intrawafer and interwafer film thickness uniformity constraints. This problem has been discussed previously for low pressure CVD reactors by Jensen and Graves.[8]

To assist efforts in optimizing operations of UHV/CVD reactors, we present a detailed mathematical model of reactant transport and deposition in the interwafer space in a multiple wafer-in-tube reactor. This model differs significantly from that of Jensen and Graves, since transport between wafers is by molecular flow. Thus, the continuum dynamical descriptions of gas flow represented by the Navier–Stokes equations must be replaced by the Boltzmann transport equation and the Kinetic Theory of Gases. In this article we present a model representation of transport and reaction within the space between the wafers which takes the form of integrodifferential equations for the flux of the reactant or intermediate species to the wafer surfaces. For established heterogeneous deposition kinetics, the model contains no adjustable parameters. We illustrate the predictive capabilities of the model for epitaxial silicon deposition from silane.

II. ULPCVD MODEL DEVELOPMENT

Consider two parallel wafers with radius R separated by a distance H as shown schematically in Fig. 1. Our config-

 0734-2101/93/11(6)/3053/9/$1.00

35 wafers in a single run, although the conditions and configuration requirements were not quantified. Greve and Racanelli show a plot indicating SiGe film thickness uniformity of approximately ±10% on six 75 mm wafers;[6] a significant portion of the observed nonuniformity may have been caused by a nonuniform axial temperature profile in the reactor. In any case, the assumption that homogeneous reactions can be neglected, as well as the other assumptions outlined above, can be modified as necessary to yield a more detailed model, and in their present form provide a basic framework through which such models could be developed.

The flux distribution to a wafer surface can be obtained by summing all possible collisions from molecules originating from the source volume or reflecting from the opposing wafer surface. Because of the symmetry inherent to the geometry, it suffices to analyze the flux distribution to one wafer face. If we further assume that the source flux is independent of θ (and θ'), then integration in the θ direction simplifies the problem in that we need subsequently consider only the radial dependence of the flux emanating from the opposing wafer (see the Appendix). For a source with flux distribution $\eta_v(y)$, the flux of molecules η_{1w} which strike wafer $n+1$ at radius r' on their first impact from the source volume differential area $2\pi R\,dy$ is

$$\eta_{1w}(r') = \int_0^H \eta_v(y) Q(r';y) 2\pi R\,dy, \tag{1}$$

where $Q(r';y)$ is the geometrically dependent transmission probability between the areas $2\pi R\,dy$ and $2\pi r'\,dr'$. For a uniform source flux, η_v can be moved outside the integration operation, and an analytical expression for the integral can be found. Meyerson and Olbricht[15] have previously developed and solved an equivalent expression to predict deposition profile uniformity for the unity reaction probability case. For most practical CVD chemistries, sticking factors are well below unity and re-emission from the opposing wafer surface must be taken into account.

The flux η_{2w} to wafer $n+1$ from molecules experiencing their second impact must emanate from the opposing wafer surface

$$\eta_{2w}(r') = \int_0^R \eta_{1w}^{L}(r) Q(r';r) 2\pi r\,dr, \tag{2}$$

where $Q(r';r)$ is the geometrically dependent transmission probability between the areas $2\pi r'\,dr'$ and $2\pi r\,dr$ and $\eta_{1w}^{L}(r)$ is the flux of molecules leaving from the area $2\pi r\,dr$ which struck that area on their first impact. Derivation of the transmission probability is described in the Appendix. The flux leaving a surface can be related to the flux striking the surface by the reactive sticking coefficient (RSC) S according to

$$\eta_w^{L} = (1-S)\eta_w \tag{3}$$

since the probability that a molecule will desorb without reacting upon collision is $1-S$.

If the accounting procedure initiated above is continued indefinitely to include all possible collisions, we can then sum to obtain the total flux of molecules striking wafer $n+1$ at r, independent of the number or sequence of previous collisions:[16]

$$\eta_w(r') = \int_0^H \eta_v(y) Q(r';y) 2\pi R\,dy + \int_0^R [1-S(r')]\eta_w(r') Q(r';r) 2\pi r'\,dr', \tag{4}$$

where we have taken advantage of the symmetry of the problem to replace $\eta_w(r)$ with $\eta_w(r')$. Note that in the general case, S is a function of flux and therefore of radial position on the wafer. Only for the special case in which the reaction is first order is the sticking coefficient independent of flux.

For multicomponent reaction systems, Eq. (4) is written for each reactive species. The set of equations are coupled through the sticking coefficient S, which may depend on the fluxes of all species present. These equations may be solved iteratively to determine the steady flux distributions to the wafer surface using the transmission probabilities given in the Appendix if sticking coefficients are known or can be estimated. In the absence of reaction ($S=0$), one finds the expected result that the flux is spatially uniform and equal to η_v.[11] For nonzero S, the deposition rate profile G can be obtained from

$$\frac{\partial T}{\partial t} = G(r') = vS(r')\eta_w(r'), \tag{5}$$

where T is the film thickness, t is time and v is the volume added to the film per reaction event.

One can make the governing equations dimensionless by choice of appropriate reference values to show that, for a single reactant deposition chemistry, only two dimensionless variables completely determine the deposition rate profile. These parameters are the reactive sticking coefficient $S(\eta_v)$ evaluated at the nominal source flux conditions and the wafer separation to wafer radius H/R. For more complex deposition chemistries, the inclusion of each additional reactant yields an additional dimensionless parameter equal to the nominal RSC for that species.

III. REACTIVE STICKING COEFFICIENTS

Buss *et al.*[17] have measured reactive sticking coefficients for silane on polycrystalline silicon using molecular beam techniques (effective pressures from 10^{-5} to 10^{-3} Torr) and a low pressure (3×10^{-3}–0.3 Torr) continuous flow cold wall microreactor. These experiments were performed in the same pressure range explored in our simulations, and for this reason we chose to use their data rather than other available data obtained at higher pressures (e.g., Refs. 18 and 19). Of course, the quantitative validity of the model predictions is dependent on the validity of the RSC expressions. Measured RSCs for silane ranged from 5×10^{-5} to 4×10^{-3} and were found to be a complex function of substrate temperature and incident reactant flux, and independent of hydrogen partial pressure. The purity level of the silane was not reported. Gates *et al.*[20] measured the RSC for ultrapure silane in UHV using thermal de-

experimental evidence to support the idea that silane dissociative adsorption is reversible. However, if one assumes dissociative adsorption of silane through a weakly bound, mobile precursor state, the RSC data can be readily fit,[21] although the overall rate expression takes a different form. For the purposes of the present modeling work, the details of the mechanism are unimportant, since only the values for RSCs are required in the governing equations.

Quantitative predictions of the silicon deposition rate are generally a factor of 2–4 lower than the few values reported by Meyerson and co-workers[1–3,22] and a factor of 4–8 lower than those reported by Greve and Racanelli.[6,7] This lack of agreement could be a consequence of uncertainty in wafer temperature measurement, since all comparisons which can be made are in the activated temperature region; thus small temperature measurement errors can lead to significant errors in deposition rate estimates. A second possible cause for mismatch between the predictions and measurements could be related to the fact that the RSC measurements of Buss *et al.*[17] were made under cold wall conditions; thermal accommodation effects may have led to sticking coefficients which are lower than those that would have been obtained under hot wall conditions.

IV. NUMERICAL SOLUTION OF THE MODEL EQUATIONS

To determine the radial flux profiles for given process conditions and wafer separation to wafer radius ratio H/R, the governing integral equation (4) for silane was solved iteratively using Gauss–Legendre quadrature. No equation for hydrogen is required, even if hydrogen is used as a "carrier gas," since we assume that hydrogen does not participate in the reaction and since gases transport independently of one another in molecular flow. Two hundred quadrature points were used in all simulations. The solutions were unaffected by using a greater number of points. The solution technique was checked by verifying that in the absence of deposition (zero sticking factor) the uniform flux solution was found to better than 0.1%. Equation (5) was used to convert from flux to deposition rate.

In our simulations we assumed that the source flux η_v is not a function of axial distance down the reactor length. Rigorously speaking, this simplifying assumption is not entirely valid, since it implies that the reactant gases are in collisional equilibrium outside the wafer space. However, *for process conditions which yield low sticking coefficients*, model predictions of radial flux and deposition rate profiles are quite insensitive to the exact functional form of the source flux. This characteristic of the model solution results because at low values of S, the contribution of the first integral in equation (4) to the total flux across the wafer is relatively small, i.e., most of the flux originates from reemission from the opposing wafer and most of the molecules undergo many such collisions before reacting or leaving the wafer space.

Knudsen numbers were calculated for all conditions to insure the validity of the molecular flow assumption of the model. Most Knudsen numbers were greater than 50. The lowest Knudsen numbers estimated were ~5. This value suggests that under such conditions flow is in the transition regime. Nonetheless, we believe that the model predictions are at least semi-quantitatively correct under these conditions. We base this claim on the work of several research groups,[23,24] who used Monte Carlo simulations of molecular flow and heterogeneous deposition in features on patterned wafers to show that for Knudsen numbers as low as 1, gas phase collisions do not significantly impact predicted deposition rate profiles.

V. RESULTS AND DISCUSSION

To simplify presentation of our simulation results, we define the dimensionless deposition rate Λ as the deposition rate at radial position r relative to the rate at the wafer edge ($r=R$). The limiting value of Λ at the wafer center is a direct measure of the intrawafer film thickness uniformity. Figure 3 shows dimensionless radial deposition rate profiles versus dimensionless radial distance ξ ($=r/R$) for different values of wafer separation and silane flux at the wafer edge for a wafer temperature of 973 K. These calculations were performed for 150 mm diam wafers, but are directly scaleable to other wafer diameters through H/R. Figures 3(a)–3(c) represent the profiles for SiH_4 pressures in the annular region of 5×10^{-5}, 5×10^{-4}, and 5×10^{-3} Torr, respectively, corresponding approximately to fluxes of 10^{16}, 10^{17}, and 10^{18} molecules/cm^2 s. Nominal sticking coefficients (values evaluated at given values of silane pressure) under these conditions are 2.7×10^{-3}, 1.7×10^{-3}, and 6.8×10^{-4}, respectively. Although sticking coefficients decrease with increasing flux, deposition rates increase; nominal deposition rates are 3, 20, and 81 Å/min for the conditions of Figs. 3(a)–3(c), respectively. As expected heuristically, intrawafer uniformity degrades for given conditions as wafer separation is decreased. To improve intrawafer uniformity and/or to achieve higher wafer density packing, conditions should be chosen which yield lower sticking factors. Based on the kinetic model employed in this study, temperature should be decreased or silane pressure should be increased. For silane decomposition, greater film thickness uniformity *and* higher deposition rate can be achieved by employing higher silane pressures.

Modification of the deposition chemistry, or choice of an alternative deposition chemistry, could lead to significantly higher effective sticking coefficients and a degradation of intrawafer film thickness uniformity. For example, introduction of germane at otherwise fixed conditions[4] with the intent of depositing SiGe thin films enhances the apparent deposition rate, and hence increases the silane sticking coefficient. Substitution of disilane for silane as the source gas in Si deposition will also lead to lower deposition uniformities for otherwise equivalent conditions, since it is well known that the disilane is markedly more reactive than silane.[25] Buss *et al.*[17] measured disilane RSCs that were an order of magnitude higher than those for silane at equivalent conditions; Sawin and co-workers measured even higher RSCs for disilane.[25] For comparison purposes, model calculations for a hypothetical flux-independent RSC of 2×10^{-2} are presented in Fig. 4. The penalty in

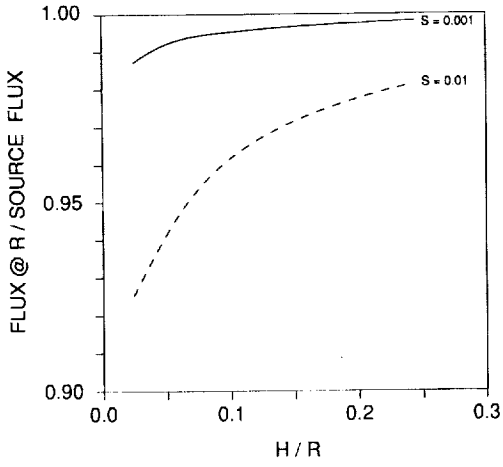

FIG. 5. Ratio of flux at wafer edge to source flux vs wafer separation to wafer radius as a function of sticking coefficient.

wafer temperature on intrawafer uniformity for the silane chemistry at a fixed wafer separation to wafer radius ratio of 1:10. We define intrawafer uniformity as the ratio of the deposition rate at the wafer center to the deposition rate at the wafer edge times 100%. This plot reflects the RSC temperature behavior illustrated in Fig. 2. At low temperature, the uniformity increases with silane flux. As temperature is increased, this dependence becomes less pronounced, until at high temperatures the uniformity becomes flux and temperature independent. It is the lower temperatures which are of greatest practical interest from a device performance viewpoint because of the material properties advantages realized for deposition performed at such conditions.

Our model calculations allow us to estimate throughput for a given uniformity constraint if the full process sequence is known or can be estimated. A complete analysis would require estimation of the following contributions to the total cycle time for processing one batch: wafer loading, reactor evacuation, heating to pretreatment temperature, pretreatment, heating or cooling to deposition temperature, deposition, postdeposition reactor evacuation, cooldown, and wafer unloading. For epitaxial silicon deposition, pretreatment consists of heating the wafers in a clean vacuum to remove the native silicon oxide; this step is thought to be critical to the success of the reduced temperature epitaxial process.[1,6] The total overhead time (time associated with steps other than actual deposition) will likely contribute substantially to the total cycle time. For this reason, high wafer packing density is a desirable goal.

To obtain a qualitative understanding of the throughput issue in UHV/CVD, we perform a partial throughput analysis by defining a "throughput number" Ξ as

$$\Xi = G(R)W, \tag{12}$$

where $G(R)$ is the deposition rate at $r=R$ (nominal deposition rate) and W is the number of wafers processed per batch. Thus, the two contributions to Ξ are equally weighted; in a full analysis the relative weighting of G and W would be dependent on the magnitude of the turnaround time relative to deposition times. For large turnaround times, W would be weighted more strongly than G. The number of wafers per batch W is given by

$$W = \frac{L}{H+\delta}, \tag{13}$$

where L is the active length of the reactor tube and δ is the wafer thickness. For the example illustrated here, we chose a value for L of 1 m and a wafer thickness of 1 mm.

Figure 7 plots throughput numbers versus temperature for various SiH_4 pressures for 150 mm wafers and an intrawafer uniformity constraint of 95%. For each of the points shown in the figure, deposition rates and number of wafers per batch are also shown. The plot clearly shows that highest throughput numbers are realized at the highest silane pressure. At a given pressure, throughput number is fairly insensitive to temperature due to the tradeoff between deposition rate and wafer spacing. As temperature is increased, deposition rate increases but wafer spacing must be increased to meet the uniformity constraint, resulting in fewer wafers processed per batch. The strongest dependence of throughput number on temperature occurs for the highest pressure.

For equivalent temperatures and pressures, it is unlikely that disilane would yield an advantage in throughput over silane. Although the higher sticking coefficients for disilane lead to higher deposition rates, these would be offset by fewer wafers per batch relative to silane. For the UHV/CVD process as currently practiced in which the overhead time is much longer than the actual deposition time, highest throughputs are realized with conditions which allow highest wafers per batch.

A complete throughput analysis is required to optimize throughput for given reactor system hardware and thin film application. Film physical and electrical properties constraints must also be met. Thus optimization for a production environment will require iterative experimental testing. Nonetheless, the free molecular flow-

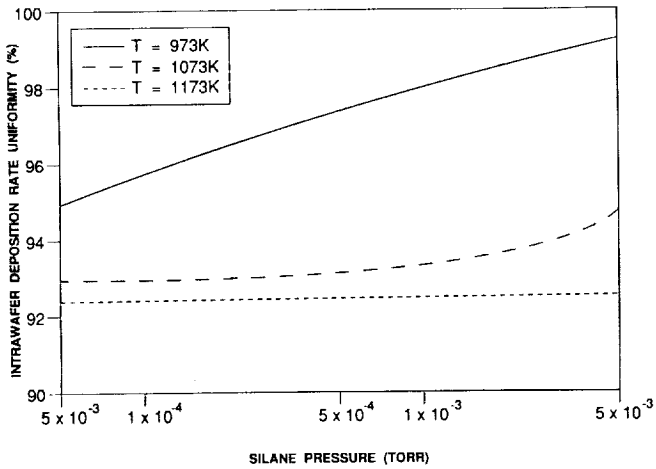

FIG. 6. Intrawafer deposition rate uniformity for epitaxial silicon deposition from silane vs silane pressure as a function of wafer temperature.

Since the transmission probability $Q(A';A)$ is defined by the following relationship:

$$\eta_{A'} = \int_A \eta_A Q(A';A)\,dA. \tag{A5}$$

Inspection of Eq. (A3) reveals that the transmission probability $Q(r';r)$ is

$$Q(r';r') = \frac{(H^2/\pi)(H^2+r^2+r'^2)}{[(H^2+r^2+r'^2)^2-4r^2r'^2]^{3/2}}. \tag{A6}$$

Note that this expression reflects the symmetry of the problem; i.e., $Q(r';r)=Q(r;r')$.

2. Source-to-wafer transmission probability $Q(r';y)$

An analogous derivation results in a similar expression for the transmission probability from the annular gas source region to wafer $n+1$; this expression is

$$Q(r';y) = \frac{(yR/\pi)(y^2+R^2-r'^2)}{[(y^2+R^2+r'^2)^2-4R^2r'^2]^{3/2}}. \tag{A7}$$

NOMENCLATURE

1. English symbols

A	area, cm^2
$\bar{c}$	mean molecular velocity, cm/s
G	film deposition rate, cm/s
H	wafer separation, mm
k	rate parameters for silane reaction, units dependent on reaction
L	active reactor length (heated zone)
n	number density, molecule/cm^3
N	silicon surface site density, sites/cm^2
Q	transmission probability, dimensionless
r	coordinate in radial direction
R	wafer radius, mm
R_{Si}	specific Si deposition rate, atoms/cm^2 s
s	line segment connecting dA and dA'
S	reactive sticking coefficient, dimensionless
t	time, s
T	film thickness, cm
W	wafers per batch
x	coordinate in axial direction
y	$H-x$

2. Greek symbols

δ	wafer thickness, mm
η	flux to a surface, molecules/cm^2 s
θ	coordinate in angular direction
Λ	dimensionless deposition rate, $G(r)/G(R)$
ν	volume added to growing film per reaction event, cm^3
ξ	dimensionless radial distance, r/R
Ξ	throughput number
ϕ	fractional coverage of adsorbed silylene
D	angle formed by s and normal to A

3. Superscripts and subscripts

v	signifies flux from source gas volume
w	signifies flux associated with a wafer surface
ι	signifies flux leaving a wafer surface
$'$	distinguishes between different areas

[1] B. S. Meyerson, E. Ganin, D. A. Smith, and T. N. Nguyen, J. Electrochem. Soc. **133**, 1232 (1986).
[2] B. S. Meyerson, Appl. Phys. Lett. **48**, 797 (1986).
[3] B. S. Meyerson, F. K. LeGoues, T. N. Nguyen, and D. L. Harame, Appl. Phys. Lett. **50**, 113 (1987).
[4] B. S. Meyerson, K. J. Uram, and F. K. LeGoues, Appl. Phys. Lett. **53**, 2555 (1988).
[5] V. Comello, Semiconductor Int. **13**, 54 (1990).
[6] D. W. Greve and M. Racanelli, J. Vac. Sci. Technol. B **8**, 511 (1990).
[7] M. Racanelli and D. W. Greve, Appl. Phys. Lett. (in press).
[8] K. F. Jensen and D. B. Graves, J. Electrochem. Soc. **130**, 1950 (1983).
[9] P. Clausing, Ann. Physik. **12**, 961 (1932); also reprinted in J. Vac. Sci. Technol. **8**, 636 (1971).
[10] T. S. Cale, J. Vac. Sci. Technol. B **9**, 2551 (1991).
[11] T. S. Cale and G. B. Raupp, J. Vac. Sci. Technol. B **8**, 649 (1990).
[12] T. S. Cale, G. B. Raupp, and T. H. Gandy, J. Appl. Phys. **68**, 3645 (1990).
[13] T. S. Cale and G. B. Raupp, J. Vac. Sci. Technol. B **8**, 1242 (1990).
[14] D. G. Coronell and K. F. Jensen, National Meeting of the AICHE, Anaheim, CA, November 1992 (unpublished), paper 30a.
[15] B. S. Meyerson and W. Olbricht, J. Electrochem. Soc. **131**, 2361 (1984).
[16] G. N. Patterson, *Introduction to the Kinetic Theory of Gas Flows* (University of Toronto Press, Toronto, 1971).
[17] R. J. Buss, P. Ho, W. G. Breiland, and M. E. Coltrin, J. Appl. Phys. **63**, 2808 (1988).
[18] W. A. P. Claassen, J. Bloem, W. G. J. N. Valkenburg, and C. H. J. van den Brekel, J. Cryst. Growth **57**, 259 (1982).
[19] D. W. Foster, A. J. Learn, and T. I. Kamins, J. Vac. Sci. Technol. B **4**, 1182 (1986).
[20] S. M. Gates, C. M. Greenlief, D. B. Beach, and P. A. Holbert, J. Chem. Phys. **92**, 3144 (1990).
[21] T. E. Zirkle, S. R. Wilson, S. Sundaram, T. S. Cale, and G. B. Raupp, J. Vac. Sci. Technol. A **11**, 905 (1993).
[22] B. S. Meyerson, B. A. Scott, and R. Tsui, Chemtronics **1**, 150 (1986).
[23] M. J. Cooke and G. Harris, J. Vac. Sci. Technol. A **7**, 3217 (1989).
[24] A. Yuuki, Y. Matsui, and K. Tachibani, Jpn. J. Appl. Phys. **28**, 212 (1989).
[25] S. K. Kulkarni, S. M. Gates, B. A. Scott, and H. H. Sawin, Surf. Sci. **219**, 13 (1990).

Appendix II:

MRS Symposium Series (1994)

THE SURFACE CHEMISTRY OF CdTe MOCVD

N15

*WEN-SHRYANG LIU AND **GREGORY B. RAUPP
*Science and Engineering of Materials Program
**Department of Chemical, Bio and Materials Engineering
Center for Solid State Electronics Research
Arizona State University, Tempe, Arizona 85287-6006

ABSTRACT

Temperature programmed desorption (TPD) studies in ultra high vacuum revealed that diethyltellurium (DETe) and dimethylcadmium (DMCd) adsorb weakly on clean Si(100) and desorb upon heating without decomposing. These precursors adsorb both weakly and strongly on CdTe(111)A, with DMCd exhibiting the stronger interaction with the surface than DETe. Dimethylcadmium partially decomposes to produce Cd adatoms; a large fraction of the excess Cd atoms desorb upon heating. In contrast, DETe desorbs without decomposing, suggesting that the rate limiting step in CdTe MOCVD on CdTe(111)A is surface decomposition of the tellurium alkyl.

INTRODUCTION

Metallorganic chemical vapor deposition (MOCVD) is a potentially attractive method for producing epitaxial CdTe or HgCdTe films since this process can in principle be scaled to large substrates and offers the potential for reasonable throughputs [1,2]. The process is more complex than competing processes such as molecular beam epitaxy (MBE) since deposition rate, film thickness uniformity and quality are complex functions of the gas phase transport and homogeneous reactions coupled with the heterogeneous reaction kinetics. Neither the precise nature of the reactions nor the relative importance of the homogeneous *vs.* heterogeneous reaction routes has not been established. Several groups have proposed that gas-phase adduct formation between the Cd and Te precursors or their decomposition fragments is an essential step in the film growth process [3,4]. Hicks has recently tested two reaction schemes using literature deposition rate data and has concluded that heterogeneous reaction steps control the initial decomposition of the precursors [5]. Gas phase reactions between hydrocarbon radicals formed through surface-adsorbed metal alkyl decomposition reactions were thought to be important in determining the gas byproduct distribution and the deposition rate through readsorption on the surface.

In this study we investigate the interaction of diethyltellurium (DETe) and dimethylcadmium (DMCd) with Si(100) and CdTe(111) surfaces using UHV thermal desorption techniques and Auger electron spectroscopy. These experiments were performed under conditions for which homogeneous reactions and byproduct readsorption are negligible, so that the results can be interpreted purely in terms of heterogeneous chemical reactions.

EXPERIMENTAL

Experiments were performed in the ultra high vacuum (UHV) chamber described elsewhere [6,7]. Si(100) substrates were chemically etched to remove surface contaminants and to form a well-defined thin oxide layer prior to introduction into the UHV chamber. The oxide layer was removed *in situ* by heating the sample in UHV to 1173 K for several minutes. Analysis of the pretreated surface with retarding field Auger electron spectroscopy (AES) showed that this pretreatment could reproducibly yield an oxygen-free surface with a trace (less than 3 atomic %) of carbon contamination. Single crystals of polished p-type (16 Ω-cm) CdTe(111) purchased from II-VI Incorporated were cleaned by immersion in E-solution [8] at room temperature for 30 s and then in boiling dithionate solution for 60-180 s prior to introduction into the UHV chamber. The sample was exposed to ultrapure hydrogen at 723 K for 30 minutes and then annealed in vacuum at 623 K for 30 minutes. Auger analyses of the pretreated surface revealed that these treatments produced a nearly stoichiometric CdTe surface with residual O and S impurities.

In a typical TPD experiment the substrate was cooled to a temperature below 180 K and then dosed with a controlled amount of DETe (Morton-Thiokol, 99.995%) or DMCd (Morton-Thiokol, 99.995%). A stainless steel syringe connected to a pressure-controlled 1 liter gas ballast reservoir was used to provide directed dosing of the source gas. Following gas exposure, samples were heated at *ca.* 15 K/s (Si) or 10 K/s (CdTe) using a tungsten filament placed behind the sample as a radiative heat source. Sample temperature was measured with a fine wire chromel-alumel thermocouple spot welded to a small tantalum spring fixed to the edge of the Si or CdTe crystal. Line-of-sight desorption flux spectra were collected using a microcomputer-controlled multiplexed VG Spectralab 1-300 amu mass spectrometer.

RESULTS

DETe and DMCd Interaction with Si(100)

The low temperature range of DETe TPD spectra from Si(100) following DETe exposure at 160 K are shown in Figure 1. The most abundant ion in the DETe cracking pattern, the parent $(C_2H_5)_2Te^+$, was tracked in these experiments. The desorption flux spectra for the lower mass ions were identical in shape and position to those for the parent ion. A single low temperature, asymmetric desorption peak at 177 K at low initial DETe coverage shifts to lower temperature with increasing coverage. Assuming first order desorption kinetics typical of molecular adsorption and desorption, and a first order pre-exponential factor of 10^{13} s^{-1}, we estimate a low coverage desorption activation energy of 43 kJ/mol. This relatively low value is consistent with a physisorption mechanism; the downshift in peak temperature with increasing initial coverage is consistent with the presence of repulsive interactions in the DETe adlayer.

Figure 2 shows the DMCd desorption flux spectra from Si(100) for three different initial DMCd coverages. In these experiments the $(CH_3)Cd^+$ ion (129 amu) was tracked since it's signal is more intense than that for the parent ion. The single desorption peak exhibits an asymmetric peak shape suggesting molecular adsorption/desorption. Unlike DETe, the

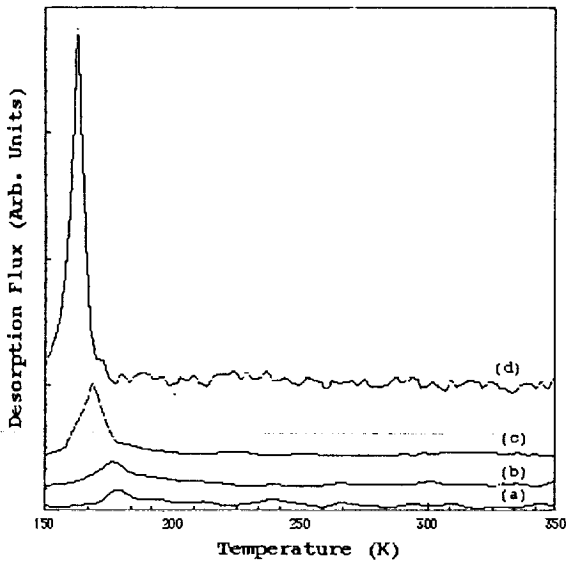

Fig. 1 Thermal desorption of DETe from Si(100) following (a) 4300, (b) 6500, (c) 9100 and (d) 15600 L DETe exposure at 160 K. (1 L = 1 Langmuir = 10^{-6} Torr-s)

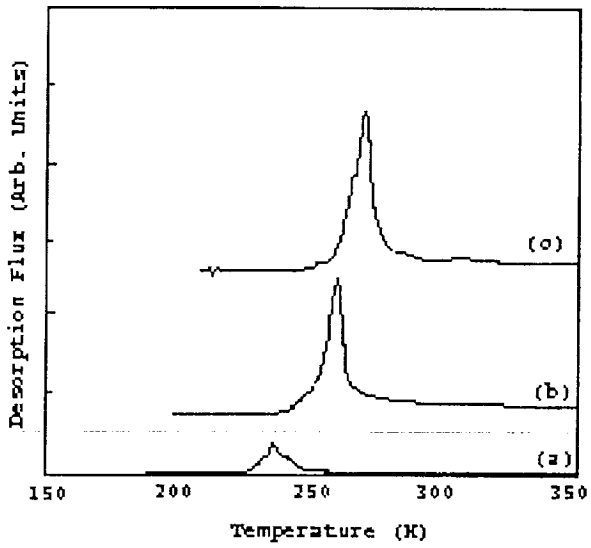

Fig. 2 Thermal desorption of DMCd from Si(100) following (a) 3900, (b) 9100 and (c) 11700 L DMCd at 180 K.

desorption peak maxima shift to a higher temperature with increasing initial coverage, suggesting the presence of attractive interactions between adsorbed DMCd molecules. The estimated desorption activation energy is 57 kJ/mol at low coverage, indicating a stronger interaction between DMCd and Si than between DETe and Si.

DETe and DMCd Interaction with CdTe(111)

The TPD spectra of DETe from the CdTe(111)A surface shown in Figure 3 contain two distinct desorption peak maxima - a narrow, intense peak at approximately 260 K and a broad, less intense peak at about 410 K. The asymmetric shape and nearly invariant peak temperature of the low temperature state are characteristic of first order kinetics, suggesting desorption of a weakly-held chemisorbed molecule. The broad width of the high temperature peak suggests that a distribution of strong molecular adsorption sites for DETe exist on the CdTe surface. Assuming first order kinetics and a 10^{13} s^{-1} pre-exponential factor, estimated desorption activation energies are 66 and 107 kJ/mol for the low and high temperature states, respectively. Figure 4 shows retarding field AES spectra of the surface collected during different stages of a single TPD experiment. The top curve was collected prior to DETe exposure, the middle curve after dosing at low temperature but prior to flashing, and the bottom curve after flashing to 700 K. The 1:0.9 Cd:Te ratio on the original surface decreased to *ca.* 1:3 after DETe exposure, reflecting the presence of adsorbed DETe on the CdTe surface. Following rapid heating to 700K the ratio decreased to 1:0.83. Within the experimental uncertainty caused by low Auger signal:noise, we conclude that the Cd:Te ratio returned to it's original value; *i.e.*, the data are consistent with desorption of DETe without deposition of Te. However , because of the overlap of the Cd and C peaks near 270 eV, it is unclear whether or not C was deposited on the surface.

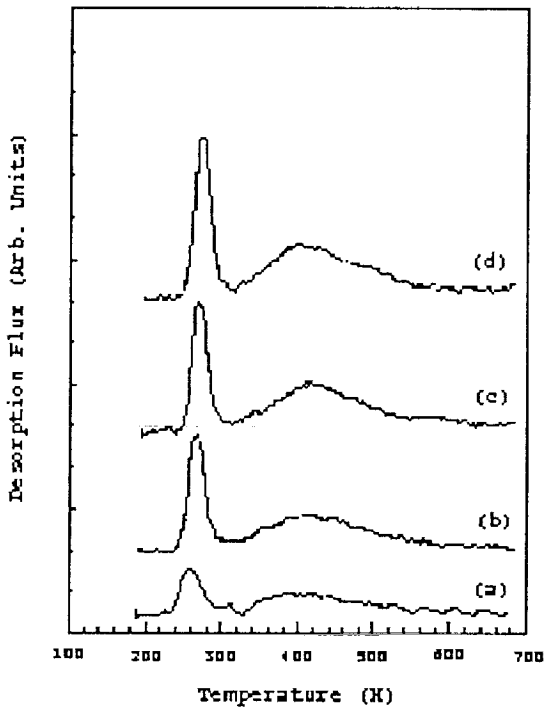

Fig. 3 Thermal desorption of DETe from CdTe(111) following (a) 10400, (b) 14300, (c) 18200 and (d) 23400 L exposure at 180 K.

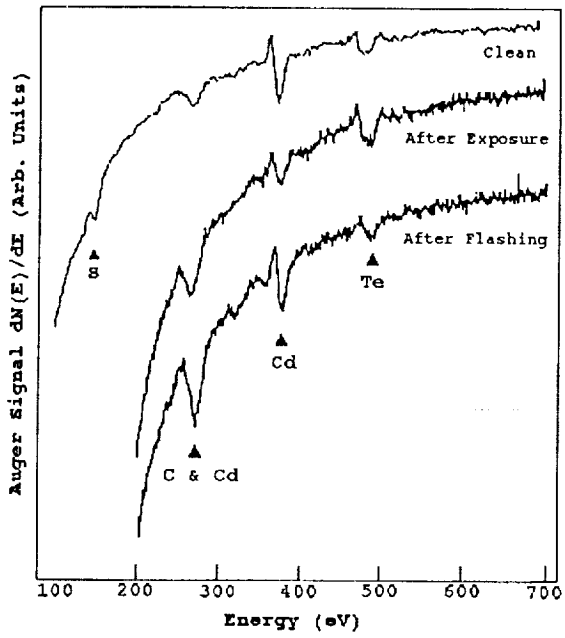

Fig. 4 AES spectra of CdTe(111) at various stages of a DETe TPD experiment.

Thermal desorption spectra of DMCd from CdTe(111)A summarized in Figure 5 show three distinct desorption features as follows: (i) a low temperature, sharp desorption peak at about 320 K which shifts to higher temperature with increased DMCd exposure, and (ii) a broad peak at about 460 K which overlaps with (iii) a second broad high temperature peak at ~ 540 K. The relative invariance or slight upshift in peak temperature with increasing initial coverage are consistent with molecular adsorption/desorption. Both the high temperature and low temperature states desorb at higher temperatures than the corresponding DETe states on CdTe, revealing a stronger interaction between DMCd and CdTe than between DETe and the CdTe surface. Estimated desorption activation energies are 80, 110 and 135 kJ/mol for the three observed states. Figure 6 shows AES spectra of the CdTe(111) surface recorded following DMCd exposure at 160 K (top curve) and following flashing to 660 K (bottom curve). Following DMCd dosing the Cd:Te ratio increased to 5:1 from the near stoichiometric initial value prior to exposure, reflecting the adsorption of DMCd. Heating to 660 K reduced the ratio to 2.6:1, suggesting that a fraction of the originally adsorbed DMCd decomposed to deposit Cd. This conclusion is supported by comparison of the apparent cracking ratio of the various ion fragments detected by the mass spectrometer during desorption of DMCd from Si(100) and from CdTe(111) as summarized in Table I. The ratio of the mono-methylcadmium to dimethylcadmium ion is essentially identical for the two surfaces, but the signal corresponding to Cd ions is significantly higher for experiments performed with the CdTe surface. On the basis of these measurements in conjunction with the AES characterization of the surface, we conclude that DMCd readily decomposes on CdTe to produce a Cd-rich surface, and that a fraction of these excess Cd atoms desorb into the gas phase upon heating.

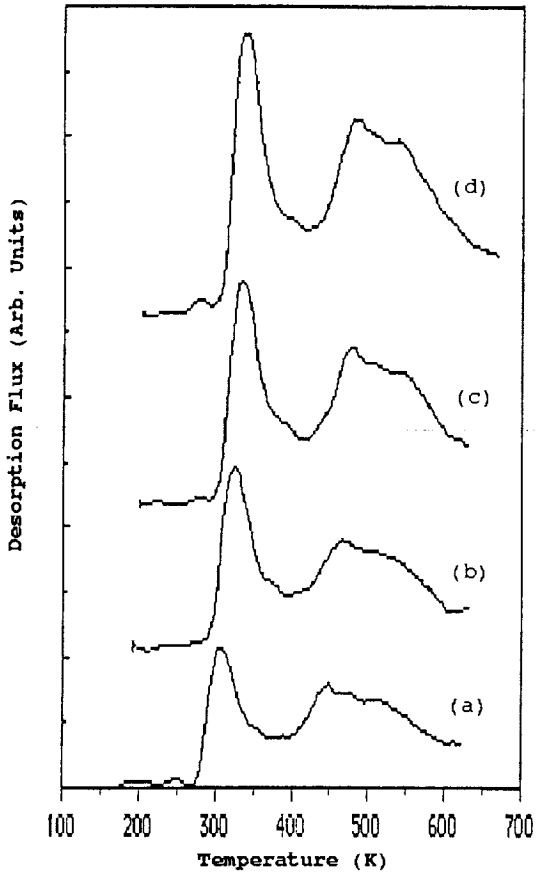

Fig. 5 Thermal desorption of DMCd from CdTe(111) following (a) 10400, (b) 14300, (c) 18200 and (d) 22000 L DMCd exposure at 180 K.

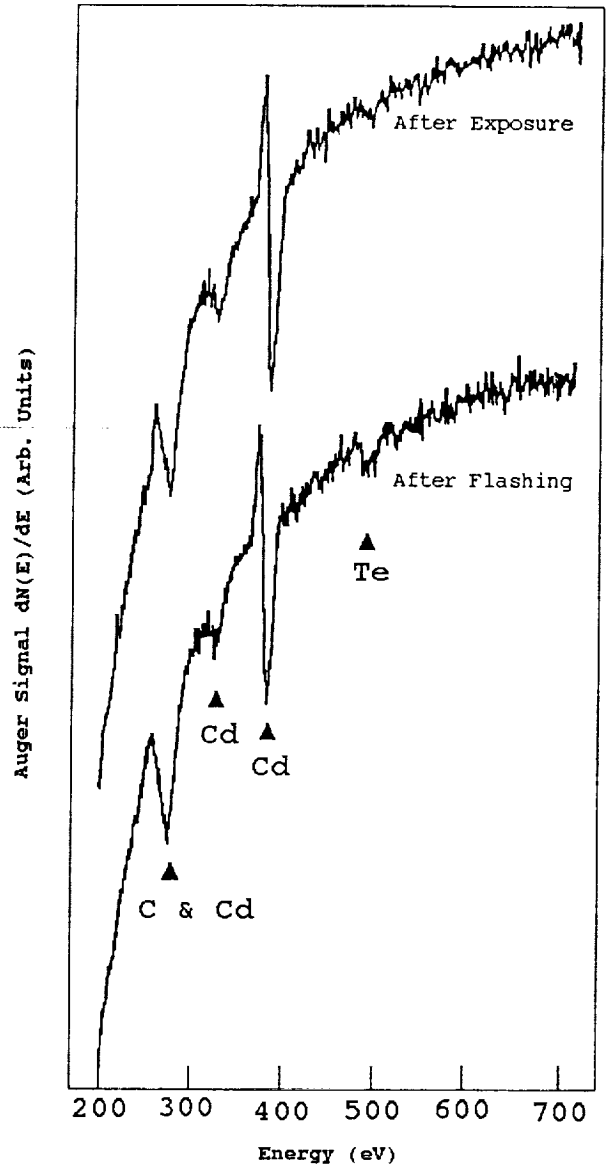

Fig. 6 AES spectra of CdTe(111) at different stages of a DMCd TPD experiment.

TABLE I. Comparison of the Apparent Ion Intensity Patterns of DMCd Desorbed from Si and CdTe

Mass:charge ratio (amu)	Ion Fragment	DMCd / Si(100)	DMCd / CdTe(111)A
114	Cd^+	4.10	9.56
129	(CH_3)-Cd^+	2.50	2.44
144	$(CH_3)_2$-Cd^+	1.00	1.00

DISCUSSION AND CONCLUSIONS

High metal alkyl exposures (thousands of Langmuirs) were required to achieve a significant extent of adsorption on the CdTe surface, and hence the sticking factors for the source gases on CdTe(111) are low. Although the sticking coefficients could not be quantified, this qualitative finding is consistent with the low measured initial sticking coefficients for dimethylcadmium and dimethyltellerium on GaAs(100) of 7×10^{-3} and 3×10^{-5}, respectively [9]. Liu *et al.* [10] extracted a sticking factor for DMCd and DETe of 1.5×10^{-4} from deposition rate data on CdTe(100). In spite of it's low sticking probability, DMCd readily decomposes on CdTe with little or no activation barrier to produce Cd atoms. In contrast, DETe does not decompose under the conditions of our experiments. During CdTe MOCVD, it is likely that excess Cd atoms produced through heterogeneous decomposition of DMCd desorb into the gas phase, where they may participate in homogeneous reactions above the substrate surface. It appears that the decomposition of DETe is not catalyzed by the Cd-rich surface, at least in the absence of adsorbed hydrogen [11]. Snyder *et al.* [12] have observed a near quenching of the CdTe deposition rate on the CdTe(111)A surface in an impinging jet reactor when the carrier gas was switched from hydrogen to helium. We conclude that, at least on this surface, the rate limiting step for MOCVD film growth is heterogeneous decomposition of adsorbed tellurium alkyl.

ACKNOWLEDGMENTS

We gratefully acknowledge the financial support of the National Aeronautics and Space Administration, Office of Space Science and Applications (NASA NAGW-1654).

REFERENCES

[1] T. F. Keuch, ***Mater. Sci. Rpts.*** 2(1), 1 (1987).
[2] D. W. Hess, K. F. Jensen and T. J. Anderson, ***Rev. Chem. Eng.*** 3, 97 (1985).
[3] J. B. Mullin, S. J. C. Irvine and D. J. Ashen, ***J. Cryst. Growth*** 55, 92 (1981).
[4] P. I. Kuznetsov, L. A. Zhuravlev, I. N. Odin, V. V. Shemet and A. V. Novoselova, ***Inorg. Mater. USSR*** 18, 779 (1982).
[5] R. F. Hicks, ***Proc. IEEE*** 80(10), 1625 (1992).
[6] G. B. Raupp and G. T. Hindman, in: Tungsten and Other Refractory Metals for VLSI VI, R. S. Blewer and C. M. McConica (MRS, Pittsburgh, PA, 1989) p. 231.
[7] G. T. Hindman, Ph. D. Dissertation, Arizona State University, 1989.
[8] M. Inoue, I. Teramoto and S. Takayanagi, ***J. Appl. Phys.*** 33, 2578 (1962).
[9] C. D. Stinespring and A. Freedman, ***Chem. Phys. Lett.*** 143(6), 584 (1988).
[10] B. Liu, A. H. McDaniel and R. F. Hicks, ***J. Cryst. Growth*** 112, 192 (1991).
[11] R. F. Hicks, National Meeting of the AICHE, St. Louis, MO, November 1993.
[12] D. W. Snyder, P. J. Sides and E. I. Ko, ***J. Electrochem. Soc.*** 139(7), L66 (1992).